

### 6.3 Rotational sled

This chapter will present the results of the test explained in the beginning of the main chapter for the rotational sled concept. The results can be seen in Figures 6.7, 6.8, 6.9.

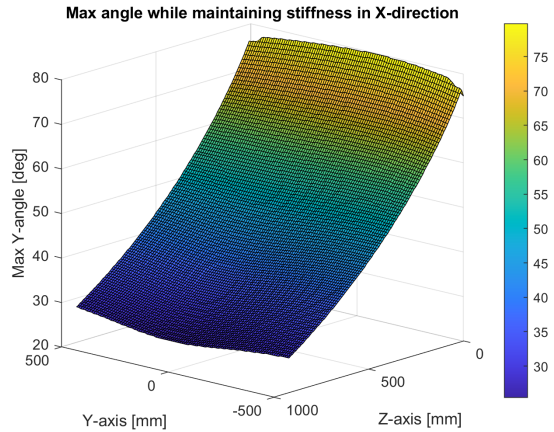


Figure 6.7: Maximum rotational angle while maintaining stiffness in X-direction

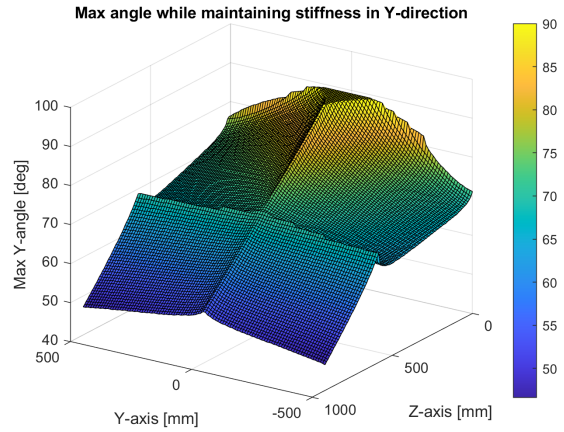


Figure 6.8: Maximum rotational angle while maintaining stiffness in Y-direction

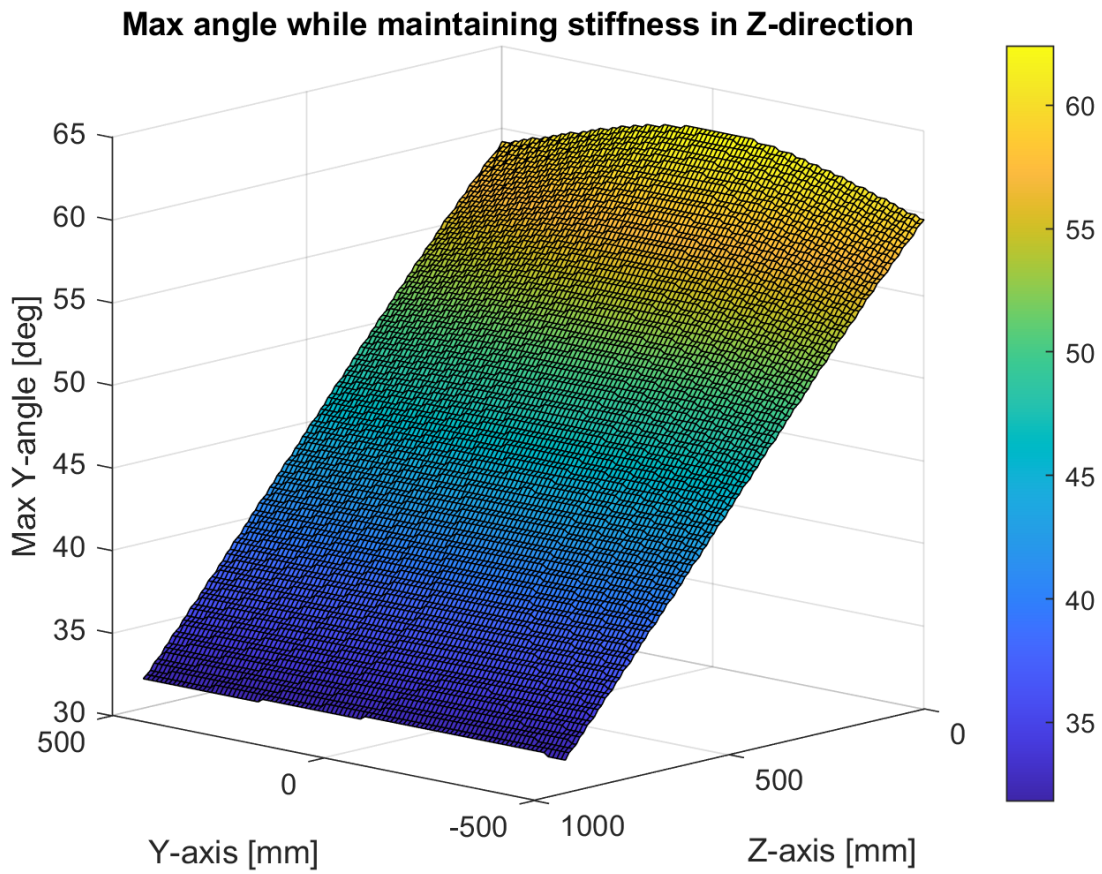


Figure 6.9: Maximum rotational angle while maintaining stiffness in Z-direction

## 6.4 Double sled

This chapter will present the results of the test explained in the beginning of the main chapter for the rotational sled concept. The results can be seen in Figures 6.10, 6.11, 6.12.

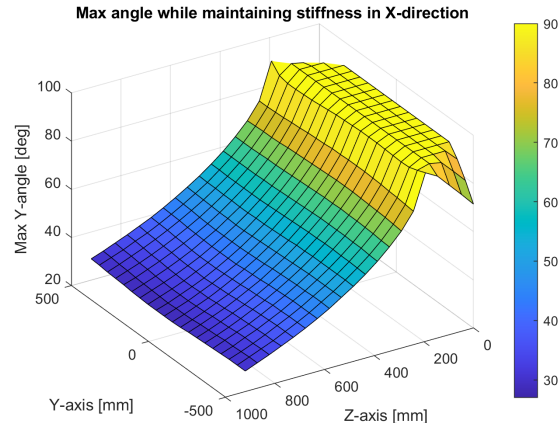


Figure 6.10: Maximum rotational angle while maintaining stiffness in X-direction

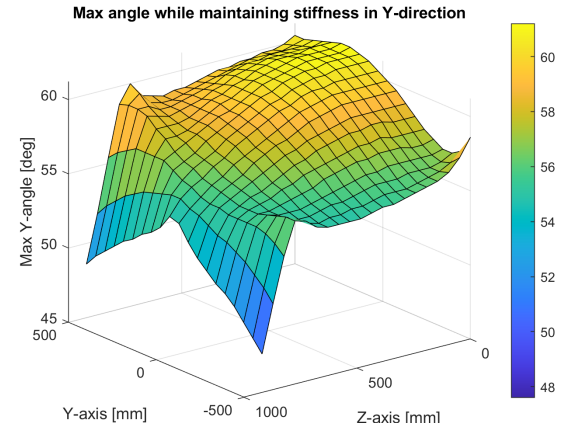


Figure 6.11: Maximum rotational angle while maintaining stiffness in Y-direction

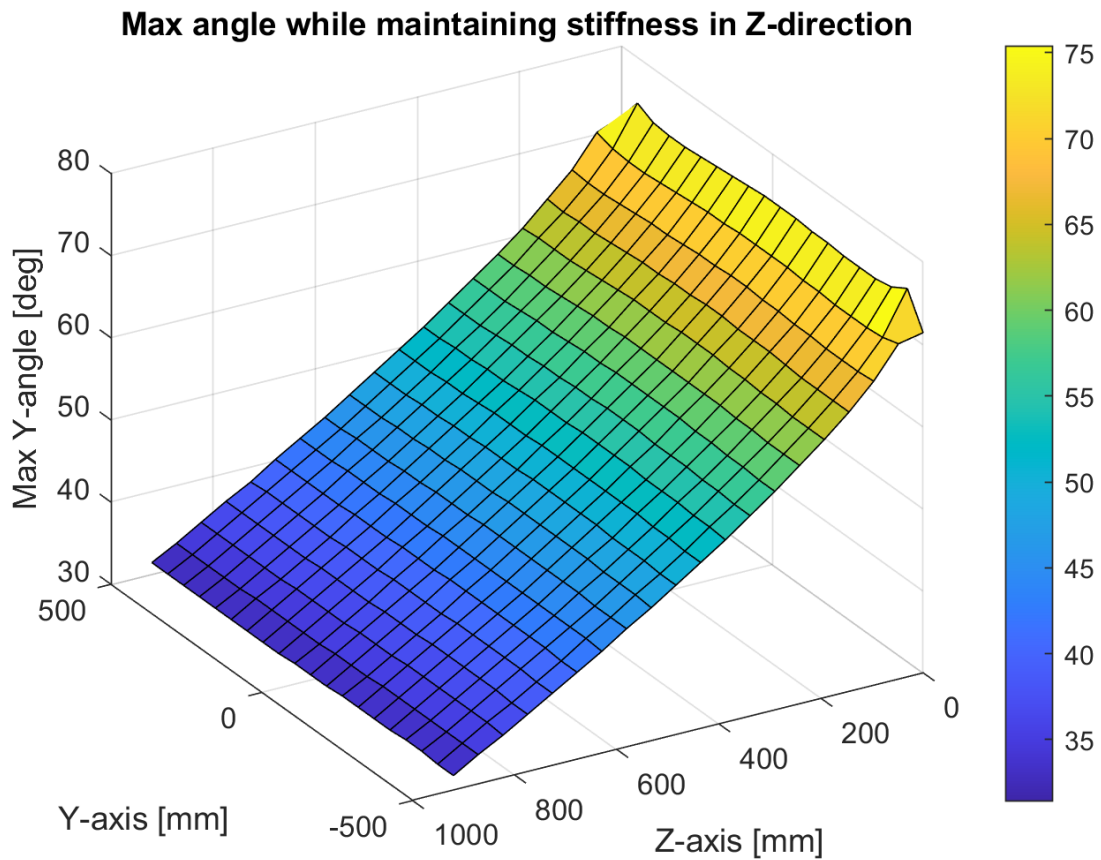


Figure 6.12: Maximum rotational angle while maintaining stiffness in Z-direction

# Chapter 7

## Final Result

In this chapter the results in Chapter 5 and 6 will be collected and refined. The most promising concept will be determined, and suggested implementation for real world potential will be suggested.

### 7.1 Choosing concept

As was found in Chapter 4, the only direction that has any possibility of being implemented without major redesign of the system is positive Y-direction rotation. Of the concepts, the mobility of every one of them with exception of the delta light concept has the same potential in this direction. Here it is necessary to look at stiffness calculations for the different concepts. For this the comparison script is used due to the overall small differences between them. It can be seen that the extending links concept and the double sled concept has very similar looking graphs, where double sled is universally better than extending links concept. Therefore extending lonks concept is dropped from further considerations.

The choice is between rotational sled concept and double sled concept. Looking at graphs for comparison stiffness of these two, it is evident that double sled is stiffer than rotational sled in X and Z-directional loads, while rotational sled is stiffer in Y-directional loads. Stiffness wise this is a tossup decision. The final decision comes between a rotational and a translational actuator. Translational actuators tend to be more rigid than a rotational actuator since the translation is larger than the rotation and thus any inaccuracies has less effect. Therefore double sled is chosen for further development.

There are unfortunately singularities in the workspace. Currently the singularity occurs for 90° the singularity occurs at approximately 436 mm height from the work table, and a Y-coordinate of  $\pm 289$  mm. The position with Y-coordinate of -289 mm can be seen in Figures 7.1 and 7.2. This singularity is caused by the line of the linkage impacting with the fastening point on the head. In Figure 7.1 the singularity is caused when the axial line of linkage D coincides with point F1 on the head. The singularity can no longer be a problem if either the control algorithm is designed to avoid the singularity position, or the system is redesigned to no longer have the singularity. In this early stage a mechanical redesign of the system is attempted.

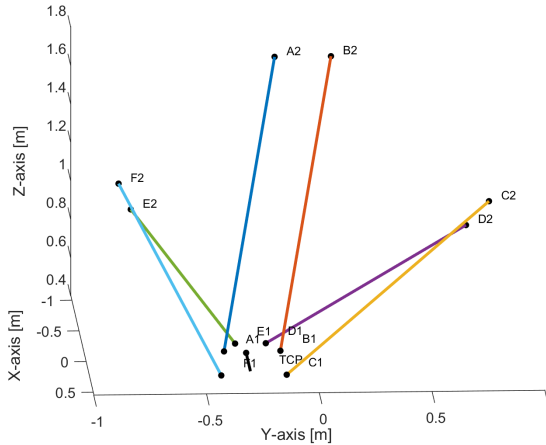


Figure 7.1: Vector model showing singularity position

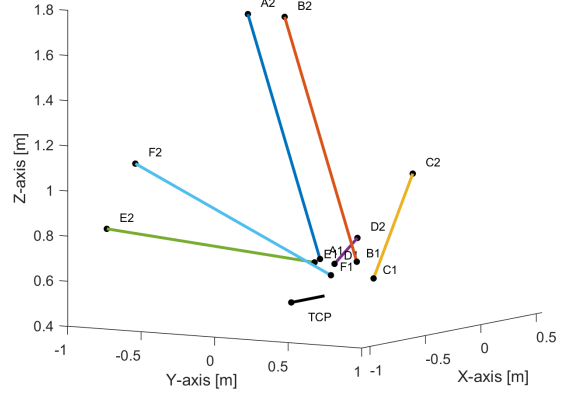


Figure 7.2: Vector model more clearly showing singularity position

## 7.2 Removing the singularities

After the choice of final concept has been made, i.e. double sled concept, next step is to attempt to remove the singularity. This is a very difficult accomplishment if the design requirement is full holonomic movement, i.e the head being able to seamlessly "sweep" between all positions and orientations here called dynamic rotation. A static orientation, i.e. the head choosing a rotation angle and sticking to it, is easier but still not possible within the deadline attached to this thesis. The only possibility to achieve some degree of functionality is to design the system to run statically for certain rotational angles. Here the angles chosen will be  $45^\circ$  and  $90^\circ$ . This would not be ideal, but would permit a certain degree of five axis machining, with room for improvement in the future. A solution is found by changing the head dimensions and linkage length to the new values seen in table 7.1. Stiffness of the linkage was also updated according to equations 5.2 and 5.3.

Value name	Change
$L_{short}$	+160 mm
$C1_x$	+100 mm
$C1_y$	+50 mm
$F1_x$	+100 mm
$F1_y$	-50 mm
$C2_y$	+50 mm
$C2_z$	-100 mm
$D2_z$	-100 mm
$E2_z$	-100 mm
$F2_y$	-50 mm
$F2_z$	-100 mm

Table 7.1: changes to the system that remedies the singularity problem

The values of table 7.1 are put into a stiffness check script for Chapter 5 and computed for  $0^\circ$ ,  $45^\circ$  and  $90^\circ$ .

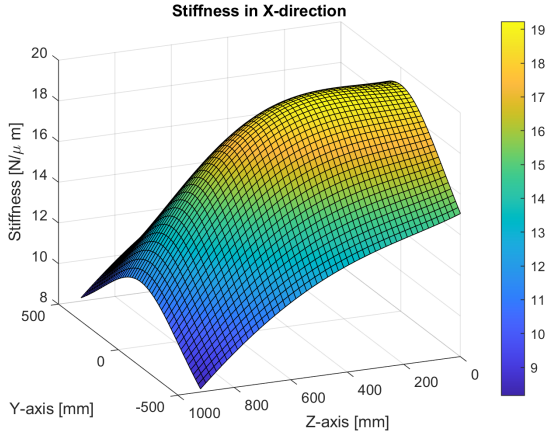


Figure 7.3: The new stiffness in X-direction at  $0^\circ$

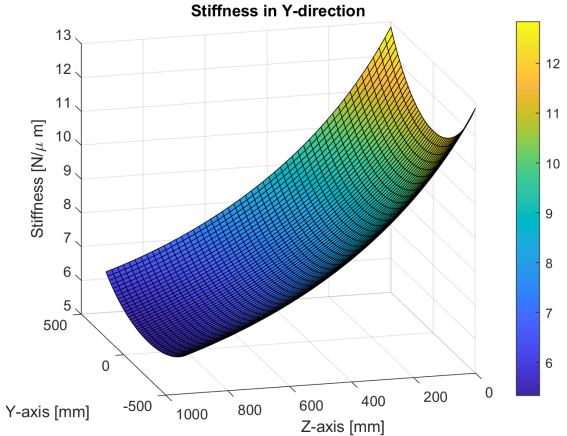


Figure 7.4: The new stiffness in Y-direction at  $0^\circ$

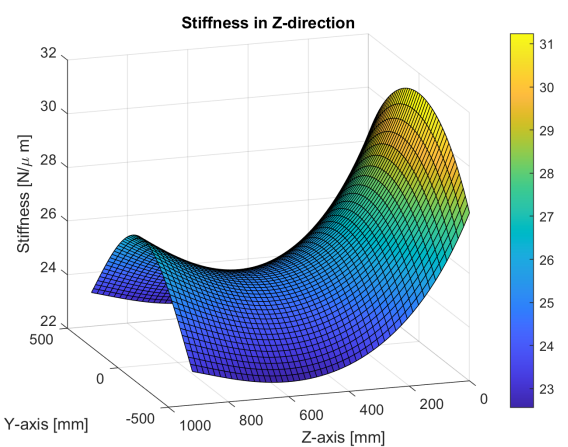


Figure 7.5: The new stiffness in Z-direction at  $0^\circ$

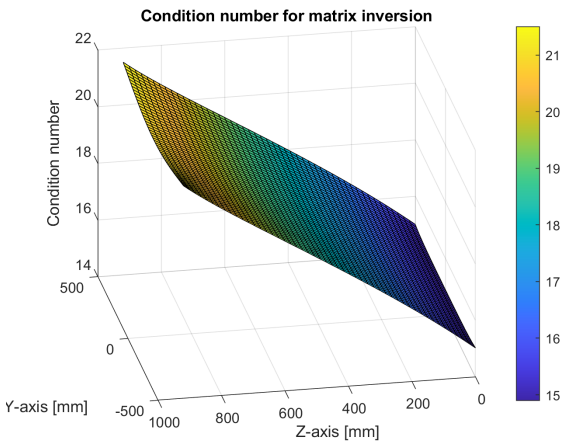


Figure 7.6: The new condition number for matrix inversion at  $0^\circ$

The stiffness results for the  $0^\circ$  rotation of the head for the new system can be seen in Figures 7.3, 7.4 and 7.5. The condition number for matrix inversion also shows a singularity free workspace, as seen in Figure 7.6. The nonzero values averaged is also quite comparable to the original system, at  $15.2 \text{ N}/\mu\text{m}$  in X-direction,  $7.9 \text{ N}/\mu\text{m}$  in Y-direction and  $25.4 \text{ N}/\mu\text{m}$  in Z-direction.

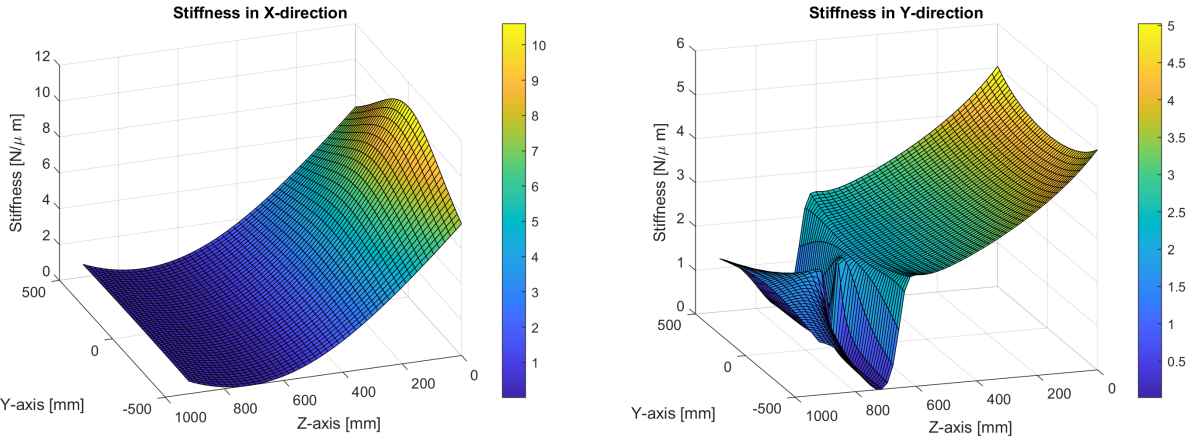


Figure 7.7: The new stiffness in X-direction at  $45^\circ$

Figure 7.8: The new stiffness in Y-direction at  $45^\circ$

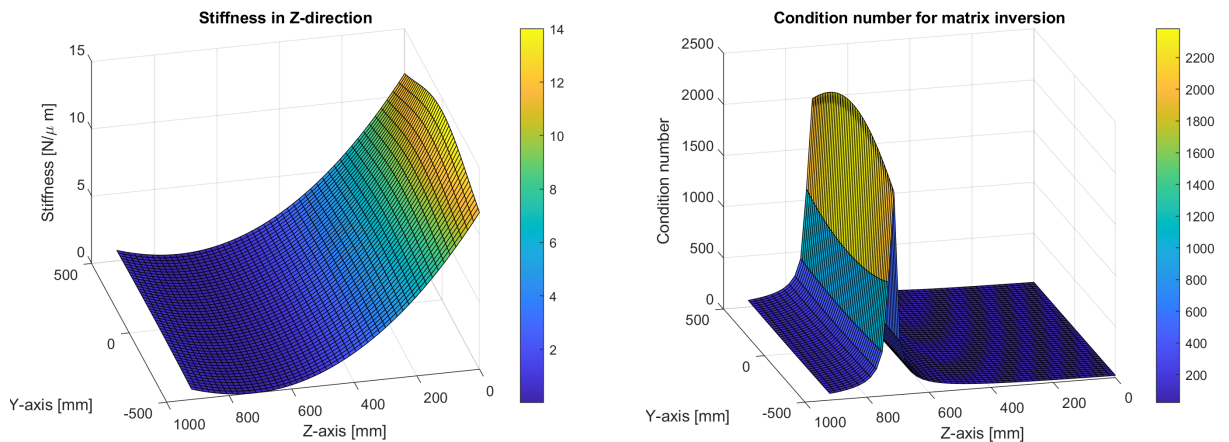


Figure 7.9: The new stiffness in Z-direction at  $45^\circ$

Figure 7.10: The new condition number for matrix inversion at  $45^\circ$

The stiffness results for the  $45^\circ$  rotation of the head for the new system can be seen in Figures 7.7, 7.8 and 7.9. The condition number for matrix inversion also shows singularities in the entire height of the workspace between 675 mm and 750 mm above the work table, as seen in Figure 7.10. This is quite acceptable due to the large height of the singularity, since the machine will work close to the bottom of the work surface for most of its run time. The nonzero stiffness values averaged are:  $2.6 \text{ N}/\mu\text{m}$  in X-direction,  $2.5 \text{ N}/\mu\text{m}$  in Y-direction and  $3.4 \text{ N}/\mu\text{m}$  in Z-direction.

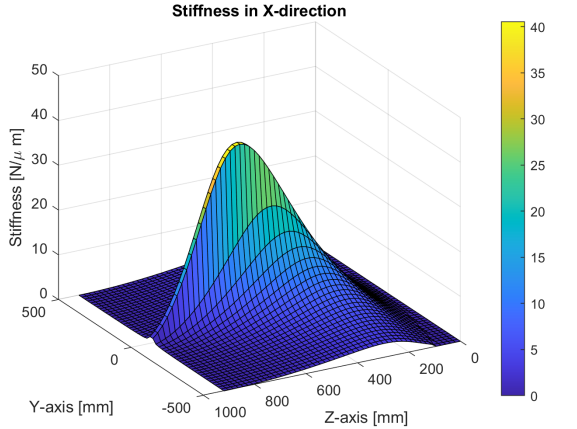


Figure 7.11: The new stiffness in X-direction at  $90^\circ$

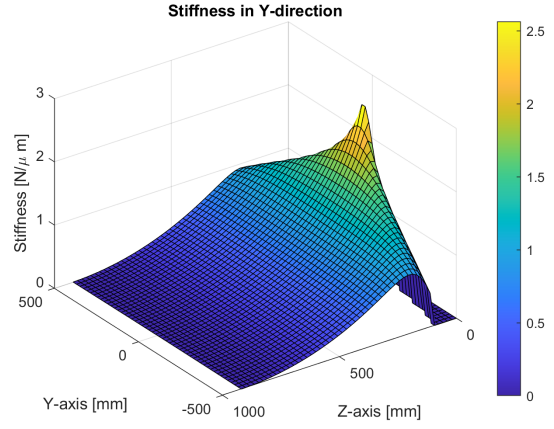


Figure 7.12: The new stiffness in Y-direction at  $90^\circ$

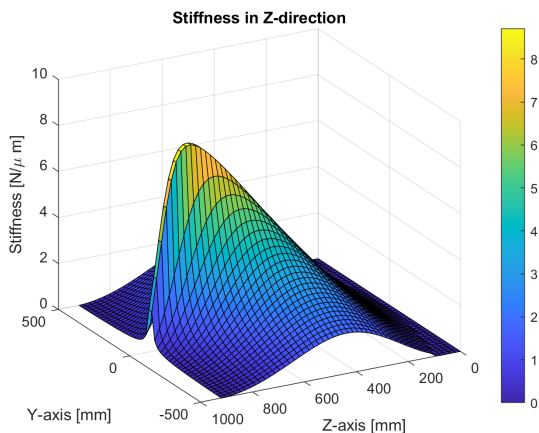


Figure 7.13: The new stiffness in Z-direction at  $90^\circ$

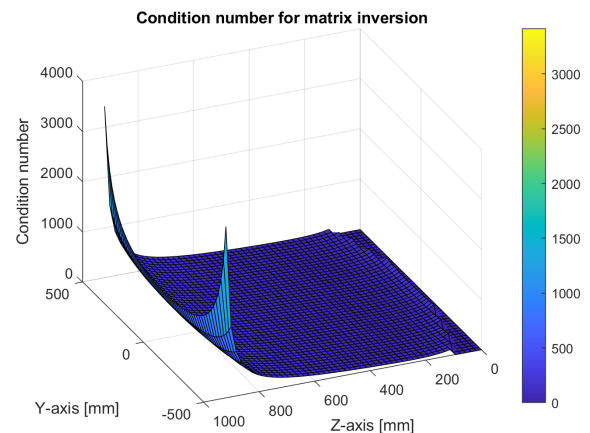


Figure 7.14: The new condition number for matrix inversion at  $90^\circ$

This new system has a functionally speaking singularity free workspace at  $90^\circ$  orientation, as can be seen in figure 7.14. The only spikes are at the very edge of the top of the workspace, which it is assumed will likely never be used at this extreme rotation of the head. The new system values also yields linkage stiffness that some might consider reasonable for the most extended position. The stiffnesses at  $90^\circ$  can be seen in Figures 7.11, 7.12 and 7.13. The values without the zero values average out to be  $4.7 \text{ N}/\mu\text{m}$  in X-direction,  $0.5 \text{ N}/\mu\text{m}$  in Y-direction and  $2.0 \text{ N}/\mu\text{m}$  in Z-direction.

The new system is also ran through the comparison test explained in Chapter 6. These graphs can be seen in Figures 7.15, 7.16, 7.17. The comparison check finds the maximum angle the new system can rotate in positive Y-direction without falling under the threshold of 30% of the stiffness of the original system. As can be seen the stiffness is quite comparable to the original double sled system. It is slightly worse in Z-direction, quite a bit worse in X-direction and quite a bit better in Y-direction. The new solution has also maintained the largest stiffness closest to the work surface, which is ideal since this is where the machine will probably spend most of its run time.

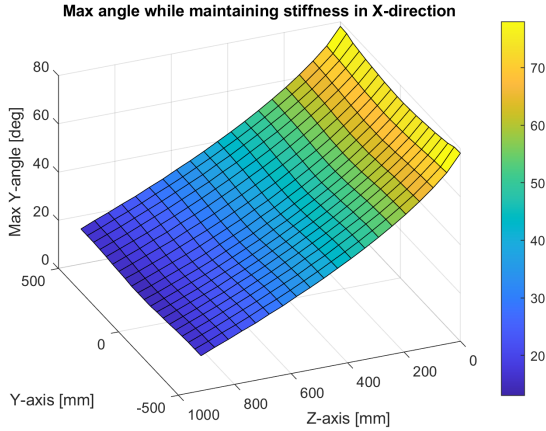


Figure 7.15: Maximum rotational angle while maintaining stiffness in X-direction for the new configuration

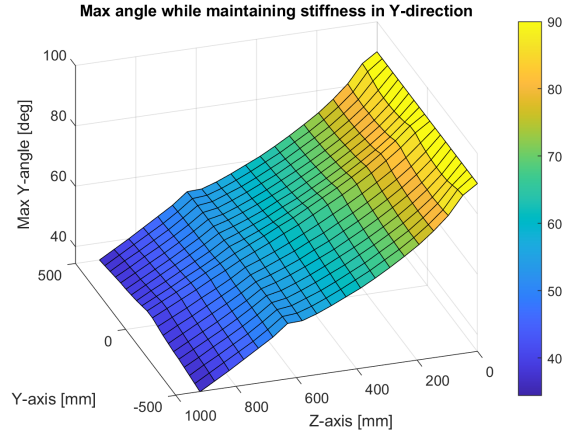


Figure 7.16: Maximum rotational angle while maintaining stiffness in Y-direction for the new configuration

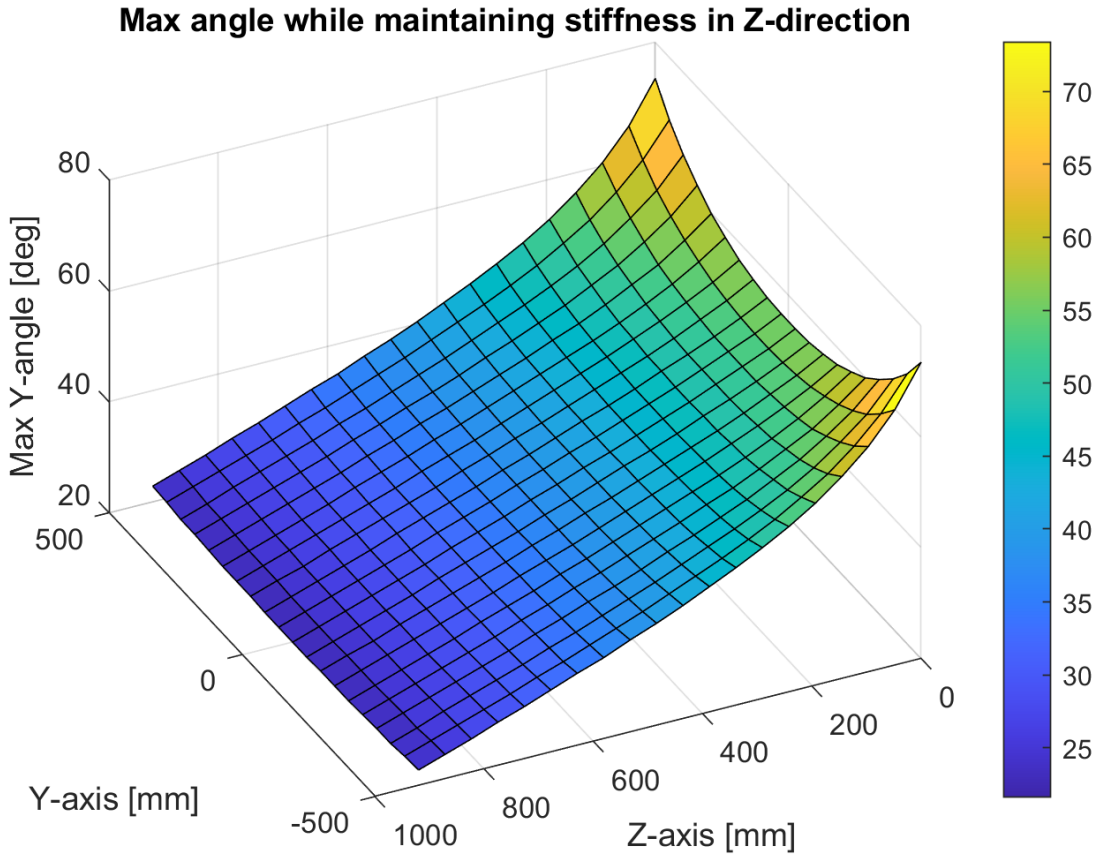


Figure 7.17: Maximum rotational angle while maintaining stiffness in Z-direction for the new configuration

### 7.3 Final implementation

This leaves the question: How do you achieve five sided machining using only the positive Y-direction rotational direction. The answer has to be a 1-DOF wrist joint. Having a  $\pm 180^\circ$  wrist joint between the points called 1 connecting the link to the head and the spindle would allow four sided machining. This can be seen in Figure 7.18. Another 5 sleds are needed to achieve full five sided machining using this concept, which can be seen in Figure 7.19.

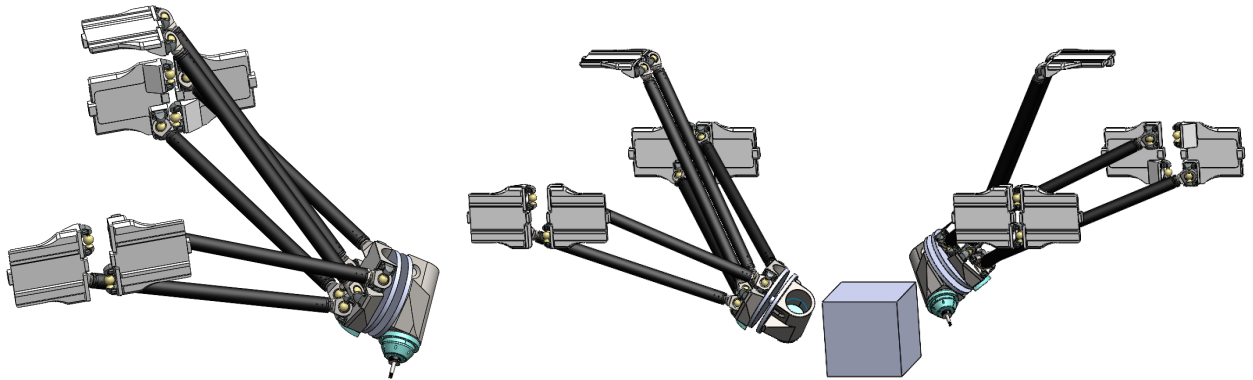


Figure 7.18: Potential solution us-  
ing the double sled concept

Figure 7.19: The potential solution implemented to achieve five  
sided machining

# Chapter 8

## Discussion

This chapter will discuss the results seen in chapters 4, 5, 6 and 7.

### 8.1 Problems with the mobility graphs

The mobility data is based on max possible movement and is probably not real world feasible. The graphs assume mathematically infinite joints in their respective degree of freedom. This is not the case in the real world. The mobility graphs represent the totality of what is possible in these three dimensions of space, but will probably have to be limited even more by real world complications. Cardan joints for example do not have infinite movement, but rather tend to have  $\pm 45^\circ$  of possible rotation before they hit the end stop. The real world capabilities of the joints chosen needs to be taken into consideration when moving forward.

### 8.2 Assumptions during stiffness calculations

The system has been assumed to be totally rigid except for the linkages. The head and body of the machine is made of metal, while the linkage is mostly made out of carbon fibre composite. So the assumption that most of the deflection is in the linkages is mostly an accurate one. There will be some give in the metal components though, so any stiffness graphs will probably over estimate the stiffness of the actual system due to this. There will also be backlash in the various joints and assemblies, which will contribute to the lowering of the overall system stiffness.

The stiffness of the linkage itself is also suspect. The tube is made of carbon fibre composite. Fibres are anisotropic, where they have the most stiffness in the axial direction of the fibre rather than the shear direction of the fibre. Therefore most carbon fibre parts are oriented such that the Mohr's principle normal stresses go in the direction of the fibres. Though having most of the forces traveling lengthwise is not the end of the considerations needed when designing with fibres. Fibres also have vastly different stiffness properties in tension vs compression. The fibres will buckle the same way a sowing thread will buckle under very little load. Of course the fibre is supported by the epoxy, so in compression the shear and the normal stiffness of the epoxy will stiffen the fibre and make it behave more rigidly than a piece of carbon fibre thread alone would. But you will still experience vastly different stiffness values for tension than for compression.

Lastly the link stiffness is suspect. The link is a female ball socket joint made out of steel. Steel is isotropic, but due to geometry it will still behave different depending on whether it is in tension vs compression. If the linkage is in compression, the contact point to the male connector will be at the base of the link, but if the linkage is in tension then the contact point will be near the end of the link. This has been shown in Figure 8.1, with blue lines showing tension force travel and red lines showing compression force travel. As can be seen the link will act quite differently depending on if it is in tension or compression, with the greatest stiffness being found in compression.

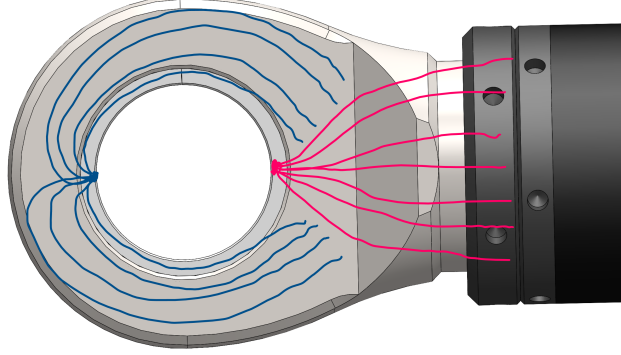


Figure 8.1: Figure showing linkage link with force lines in blue for tension and red for compression

These concepts will all change the stiffness values of the actual system. If the fibre direction varies between linkages the stiffness also varies. If the linkage is in tension or in compression this also changes the overall stiffness of the linkage. In this report the stiffness values has been kept constant to limit complexity, which is a simplification. The assumption is that the tests in this early stage of prototyping only really need to give an indication of final performance. Essentially the test is only used to compare between the different schemas. Thus even if the test is flawed, it is applied evenly among all the different concepts, and will therefore pick up on differences between them.

### 8.3 Problems with the final Implementation

The chosen solution is to have a double sled concept with a 1-DOF wrist joint at the terminus of the linkages. The chosen concept can operate without singularities in the  $45^\circ$  orientation, and has two singular positions in the  $90^\circ$  orientation. The new system of Chapter 7 combined with the double joint and wrist joint solution would have a singularity free  $90^\circ$  orientation, but would have a height layer with singularities in the  $45^\circ$  orientation.

None of these two sets of joint positions have the ability to "sweep" through the workspace, i.e. move holonomically between all orientations and positions. This will negatively impact the markets that this machine can be sold to, since ideally the machine should be able to sweep in the entirety of its workspace. This has not been achieved here, but is largely a matter of choosing joint positions that avoid singularities in the workspace. This would allow the machine to be used to machine flowing curves holonomically, meaning that airplane and engine manufacture is a distinct possibility. As is, the machine proposed can operate almost fully while locked in the orientation chosen. This means the machine is locked to producing more standard, "blocky" architecture when used in full five-sided machining. But it can move holonomically in  $\pm 30^\circ$ , which means that the mold making industry may take an interest in the machine with the double sled concept implemented.

The next step in redesigning the machine should be to distinctly choose an industry to aim for. Different industries have different requirements for capabilities of the machine. Continuing with the general approach will very quickly become very expensive since the development needs to account for several sets of requirements of the machine. Choosing only one target will allow for greater fine tuning of the machine, instead of the general approach which has been chosen thus far. This is a necessity because there is a greater number of variables that affect the final product in the five-DOF configuration than in the three-DOF configuration.

### 8.4 Future work

This chapter will briefly itemize the path the redevelopment can take in the future.

- Look into redesign of the head to possibly be able to offer X-direction rotation that way, thereby avoiding a 1-DOF wrist joint
- Look into possibilities of combined solutions, i.e. having double sled concept implemented on east sled and extending links concept on west sled
- Find other new configurations of the double sled concept that have favorable singularity graphs for bending in positive Y-direction, and optimize for stiffness (Possibility for new master thesis)
- Look into possibilities of one or more linkages to get a more beneficial singularity distribution in the workspace (possibility for new master thesis)
- Optimize head linkage fastening points to avoid singularities for as many as possible rotational angles and positions probably using an AI model (Possibility for new master thesis). Also the optimization algorithm used in [13] can be a very useful approach here.
- Look into redesign of the head to be at an offset angle at the sled when the TCP is in the zero position, thus increasing the stiffness for certain rotational positions. Very similar to the way Metrom does it in Figure 2.16.

# Chapter 9

## Conclusions

This thesis set out to establish a basis for a future redesign of a parallel kinematic CNC machine. It has done a brief study of the current high tech of PKMs. An overview of possible joint alterations to this machine has also been conducted. Kinematic potential in the X and Y-directions have been analysed for all concepts that showed potential. Results of the kinematic equations quickly showed that a rotation in X-direction is unlikely to be accomplished without major redesign of the head to avoid linkage crashing, and even then the workspace in this orientation would be severely lowered from the current workspace. The only rotational direction that has any potential is in Y-direction. The stiffness in positive Y-direction from  $0^\circ$  to  $90^\circ$  has been analysed both in absolute values and in values relative to the original machine for all concepts. Based on stiffness results and real world feasibility the double sled concept has been chosen as the most promising direction for further development, though the rotational sled concept is a very close second.

The double sled concept has a two singular points in the workspace at  $90^\circ$ . The concept was therefore altered slightly to achieve a singularity free work space, though at the cost of the  $45^\circ$  workspace which now has an entire section of the workspace that now contains singularities. The idea is to choose one set of values depending on which market the machine is designed for, but for now both sets of system values are a possibility. Both these systems need two heads to be able to machine fully five-sided.

The end result is a machine design that has the ability to orient the TCP in  $-0^\circ + 90^\circ$  Y-direction and  $\pm unkown^\circ$  in X-direction. The rotation in X-direction will have to come from the choice of wrist joint supplier which will ultimately be chosen based on which market the machine will be sold in. The TCP can operate freely in either  $45^\circ$  or  $90^\circ$  Y-direction, but no solution has been proposed that can handle both these orientations without encountering singularities somewhere in the workspace. The solution proposed can also not move holonomically between the different orientations, and will only properly work currently being static in one orientation while in contact with the work piece. It is recommended to use the double sled concept in further development, and focus on redevelopment of the head and frame contact points to avoid singularities as much as possible. If the singularities is avoided to an acceptable degree then full five-sided holonomic operation is possible.

Future redesign has many different roads that are possible. The choice needs to be taken in regards to which industry the machine in question is aimed at appealing to. As is, the concept chosen has a broad range of possible industries it can ultimately function in, but without greater specification of the market demands no great engineering work can be undertaken. Specifying a development goal is highly recommended, as this will simplify the engineering requirements and therefore lower costs greatly.

## Appendix A

### Stiffness graphs for extending links concept

## A.1 10 Degrees

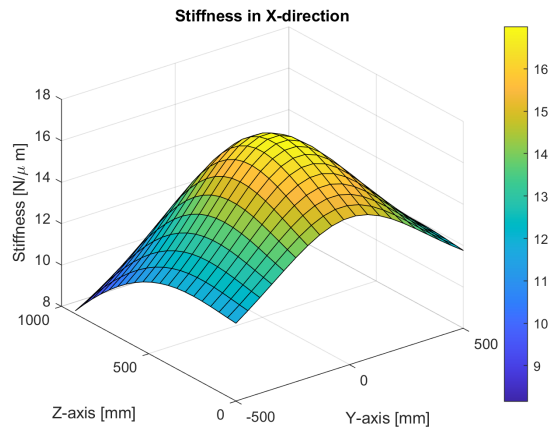


Figure A.1: Stiffness for load in X-direction for extending links concept at 10° head angle

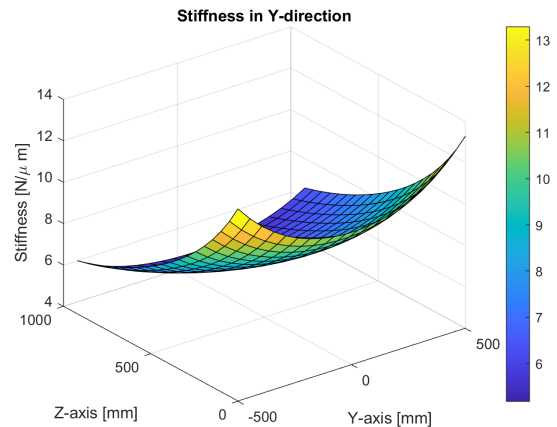


Figure A.2: Stiffness for load in Y-direction for extending links concept at 10° head angle

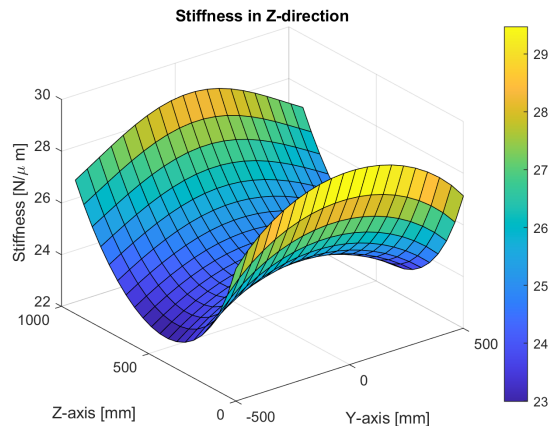


Figure A.3: Stiffness for load in Z-direction for extending links concept at 10° head angle

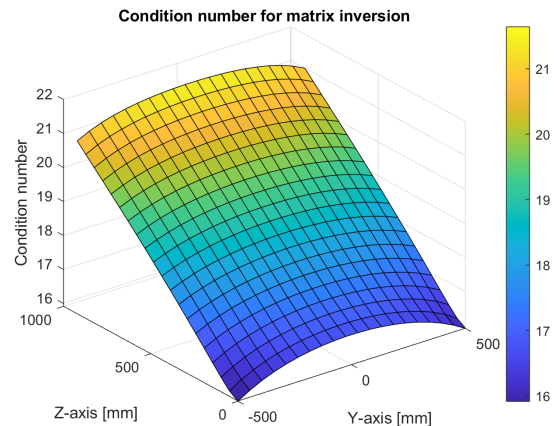


Figure A.4: Condition number for matrix inversion for extending links concept at 10° head angle

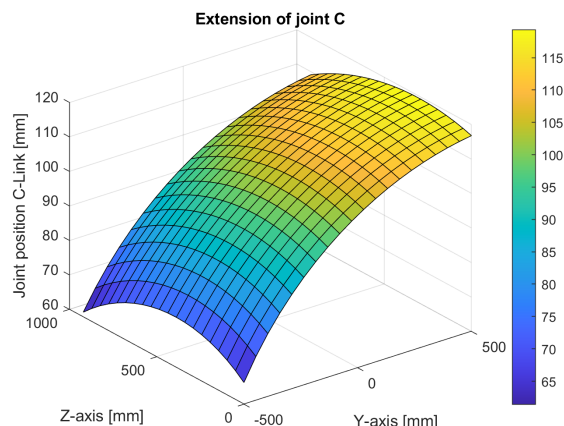


Figure A.5: Joint position at C2 for extending links concept at 10° head angle

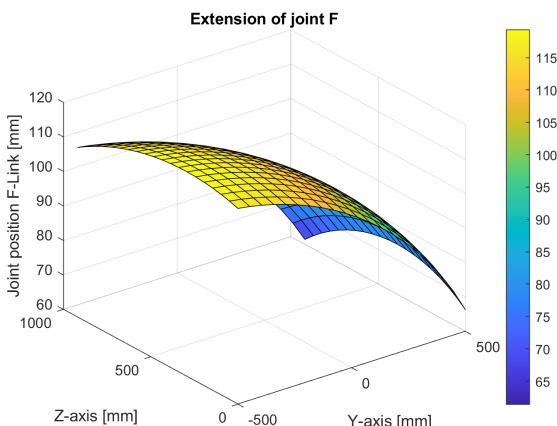


Figure A.6: Joint position at F2 for extending links concept at 10° head angle

## A.2 20 Degrees

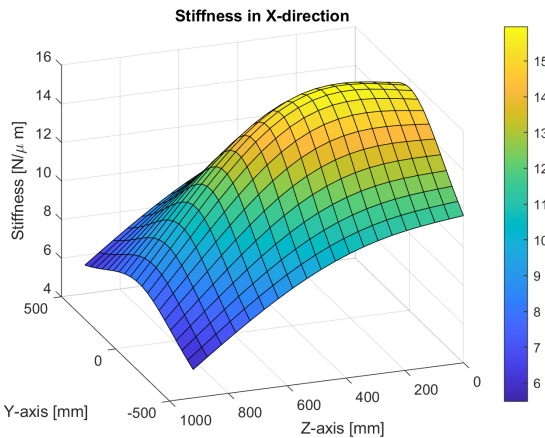


Figure A.7: Stiffness for load in X-direction for extending links concept at 20° head angle

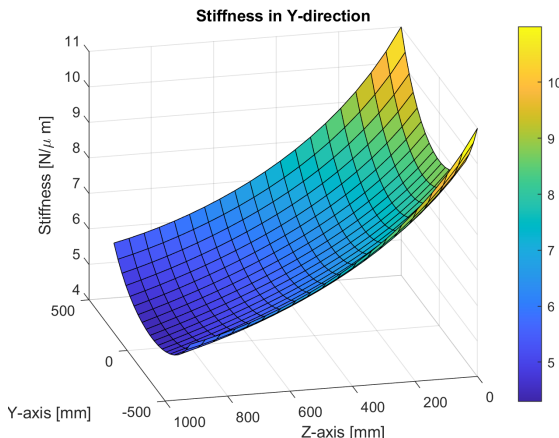


Figure A.8: Stiffness for load in Y-direction for extending links concept at 20° head angle

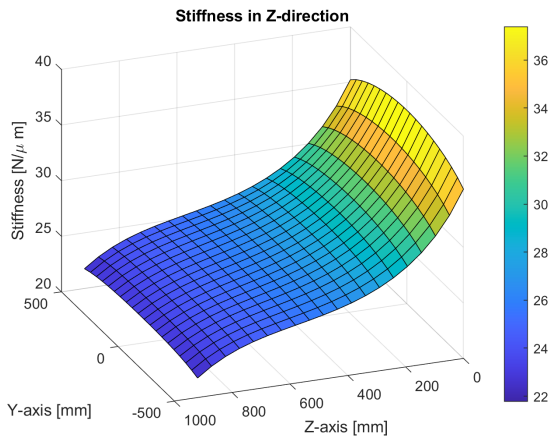


Figure A.9: Stiffness for load in Z-direction for extending links concept at 20° head angle

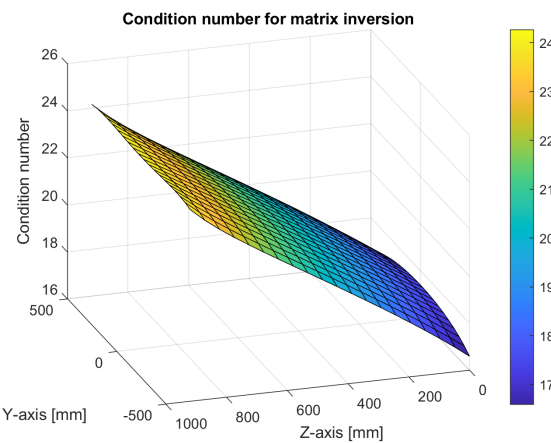


Figure A.10: Condition number for matrix inversion for extending links concept at 20° head angle

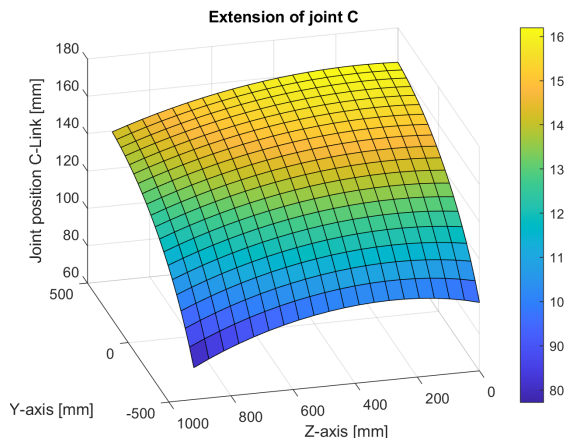


Figure A.11: Joint position at C2 for extending links concept at 20° head angle

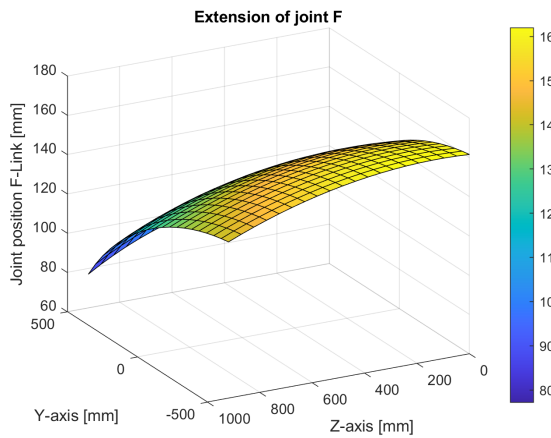


Figure A.12: Joint position at F2 for extending links concept at 20° head angle

### A.3 30 Degrees

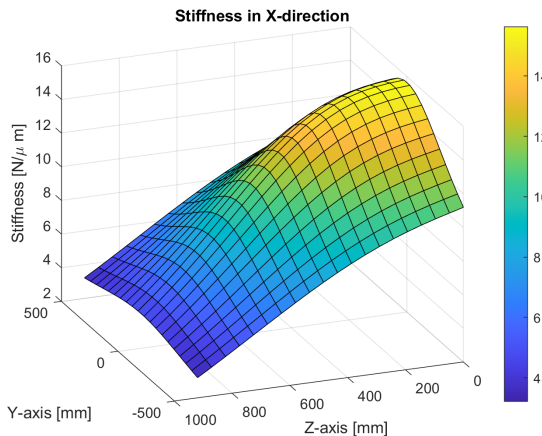


Figure A.13: Stiffness for load in X-direction for extending links concept at 30° head angle

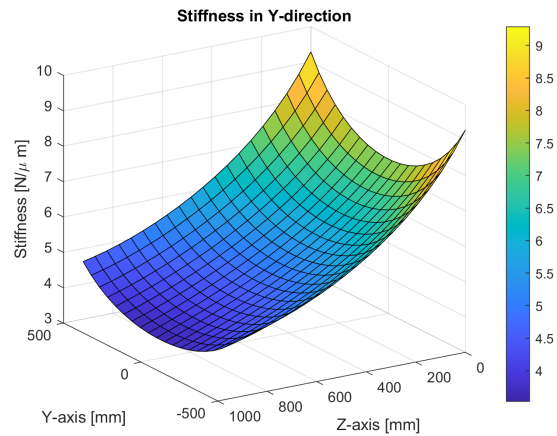


Figure A.14: Stiffness for load in Y-direction for extending links concept at 30° head angle

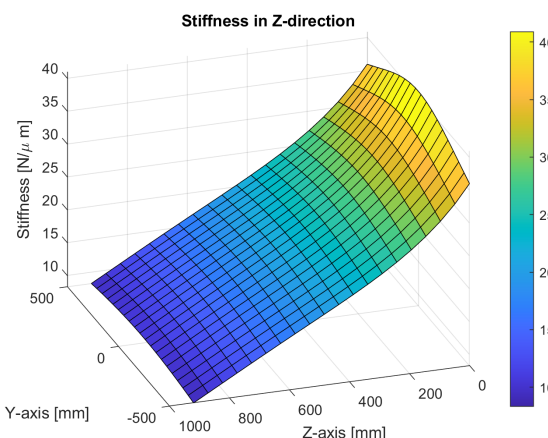


Figure A.15: Stiffness for load in Z-direction for extending links concept at 30° head angle

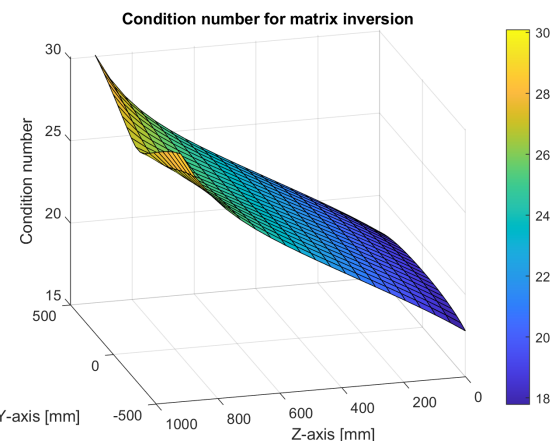


Figure A.16: Condition number for matrix inversion for extending links concept at 30° head angle

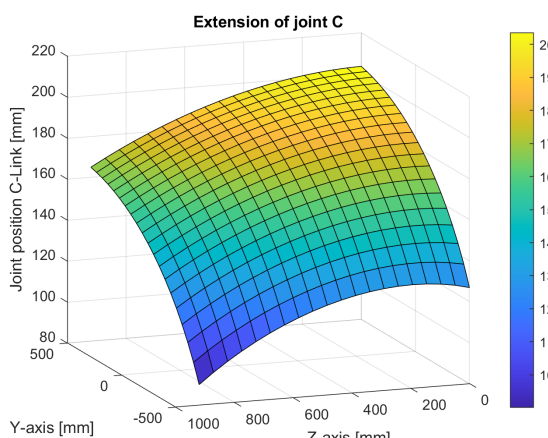


Figure A.17: Joint position at C2 for extending links concept at 30° head angle

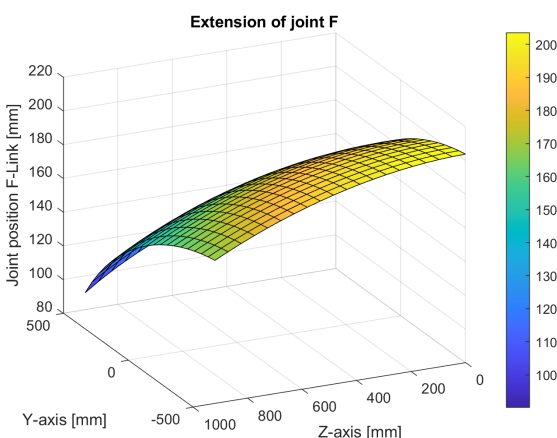


Figure A.18: Joint position at F2 for extending links concept at 30° head angle

## A.4 40 Degrees

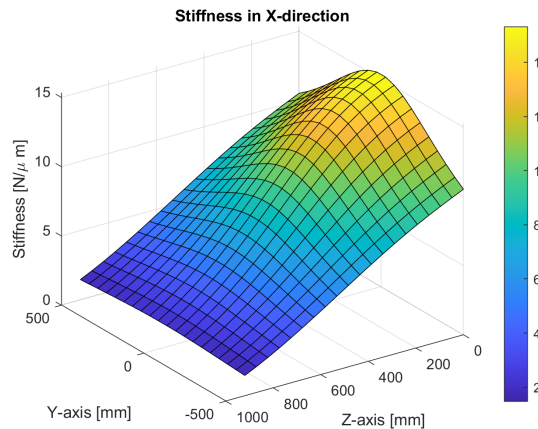


Figure A.19: Stiffness for load in X-direction for extending links concept at 40° head angle

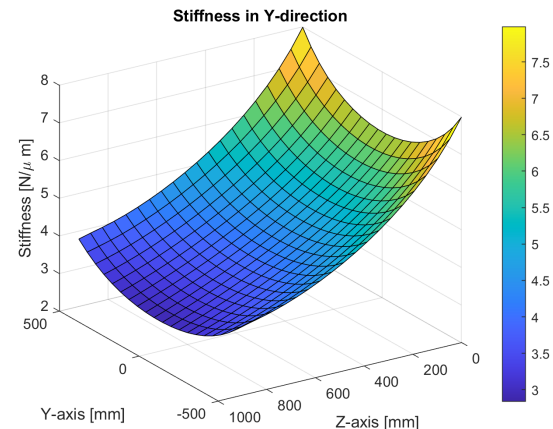


Figure A.20: Stiffness for load in Y-direction for extending links concept at 40° head angle

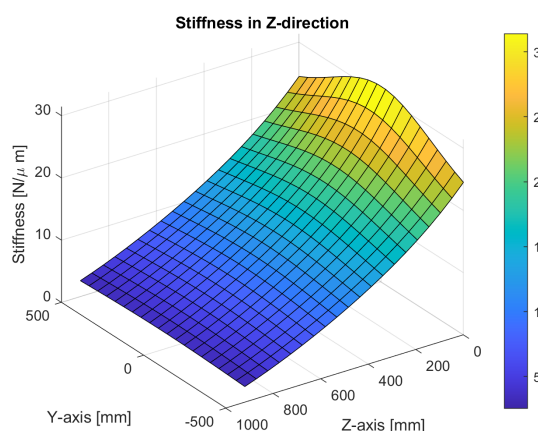


Figure A.21: Stiffness for load in Z-direction for extending links concept at 40° head angle

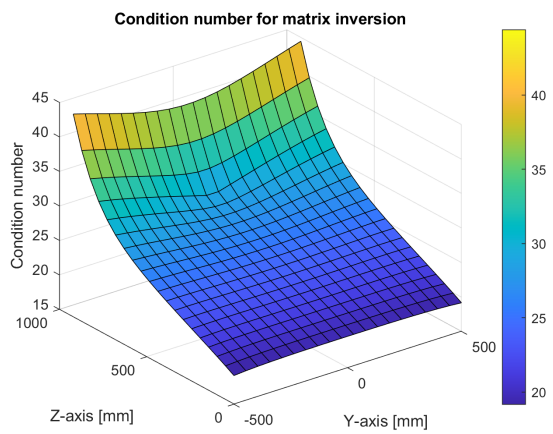


Figure A.22: Condition number for matrix inversion for extending links concept at 40° head angle

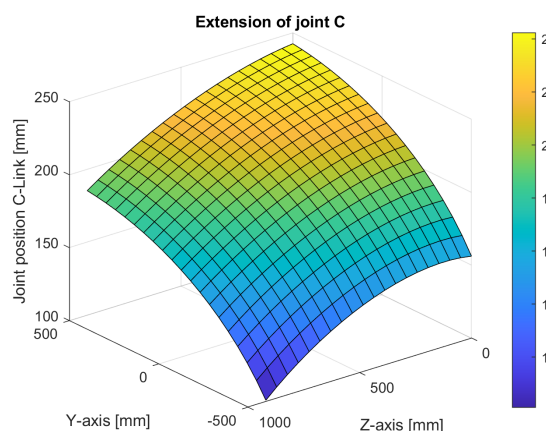


Figure A.23: Joint position at C2 for extending links concept at 40° head angle

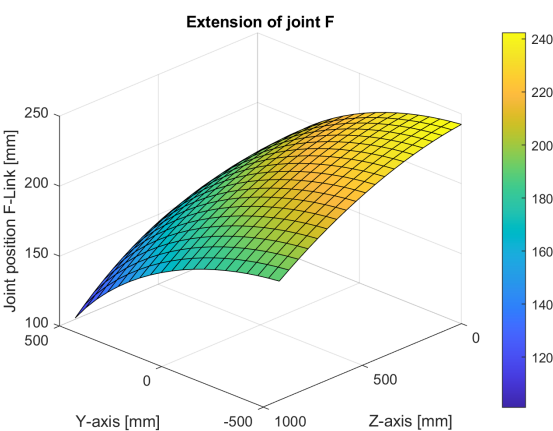


Figure A.24: Joint position at F2 for extending links concept at 40° head angle

## A.5 50 Degrees

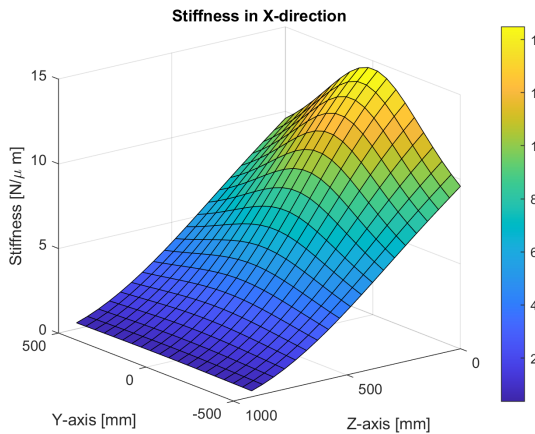


Figure A.25: Stiffness for load in X-direction for extending links concept at 50° head angle

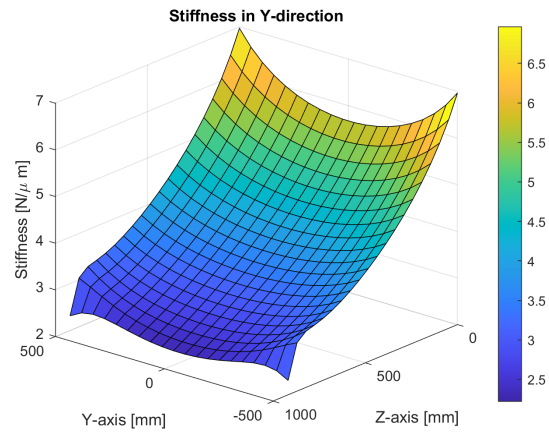


Figure A.26: Stiffness for load in Y-direction for extending links concept at 50° head angle

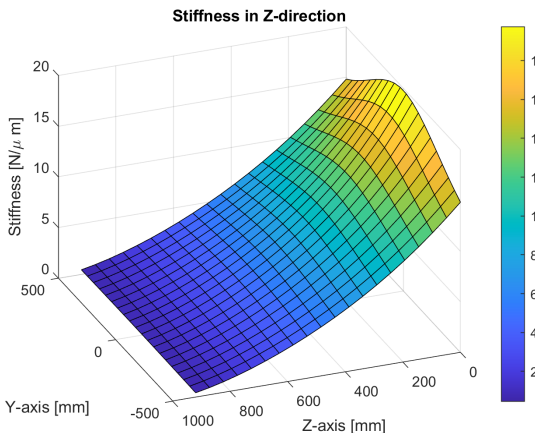


Figure A.27: Stiffness for load in Z-direction for extending links concept at 50° head angle

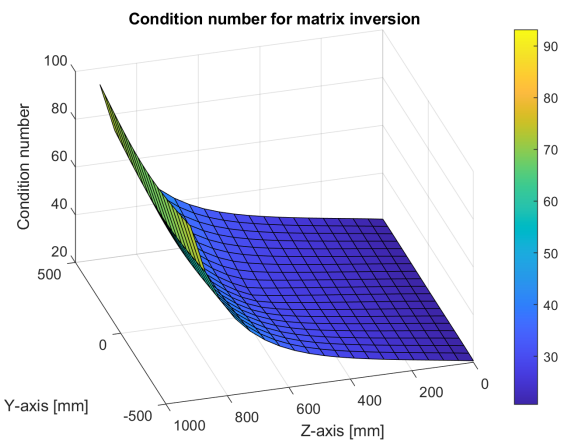


Figure A.28: Condition number for matrix inversion for extending links concept at 50° head angle

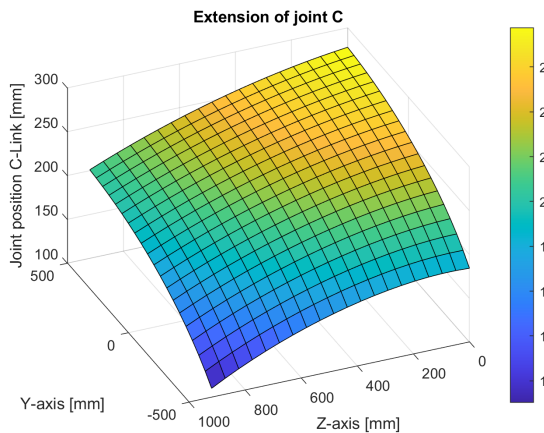


Figure A.29: Joint position at C2 for extending links concept at 50° head angle

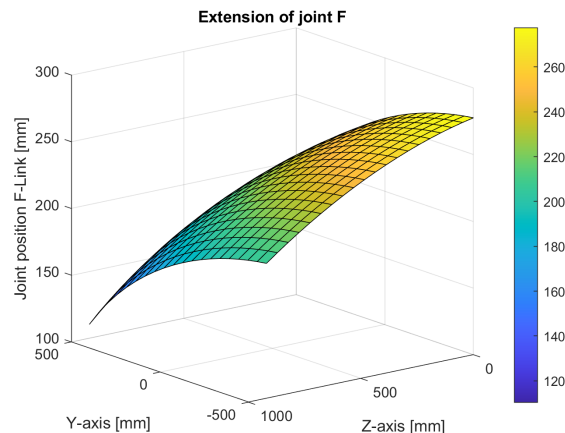


Figure A.30: Joint position at F2 for extending links concept at 50° head angle

## A.6 60 Degrees

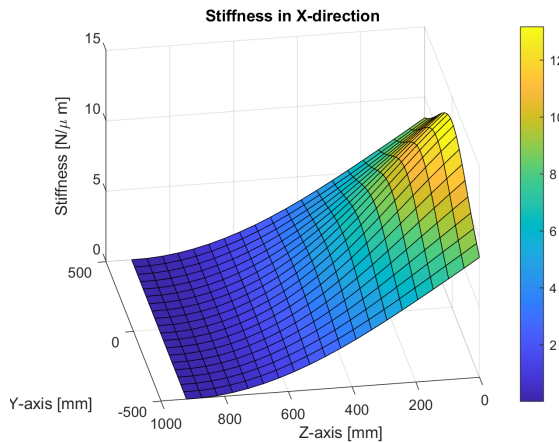


Figure A.31: Stiffness for load in X-direction for extending links concept at 60° head angle

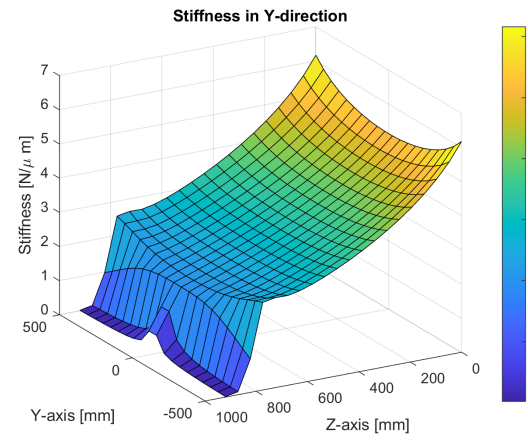


Figure A.32: Stiffness for load in Y-direction for extending links concept at 60° head angle

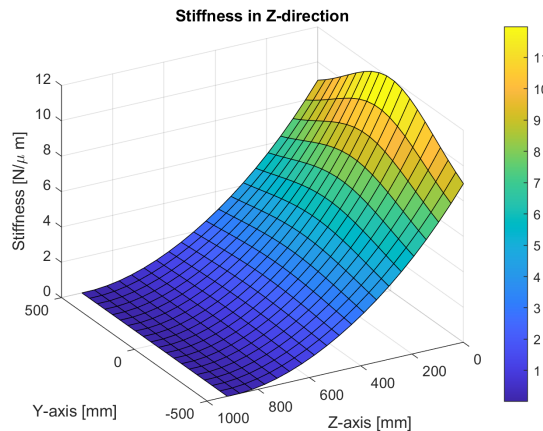


Figure A.33: Stiffness for load in Z-direction for extending links concept at 60° head angle

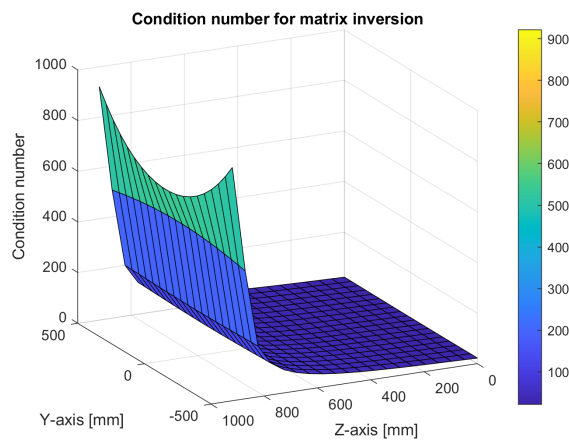


Figure A.34: Condition number for matrix inversion for extending links concept at 60° head angle

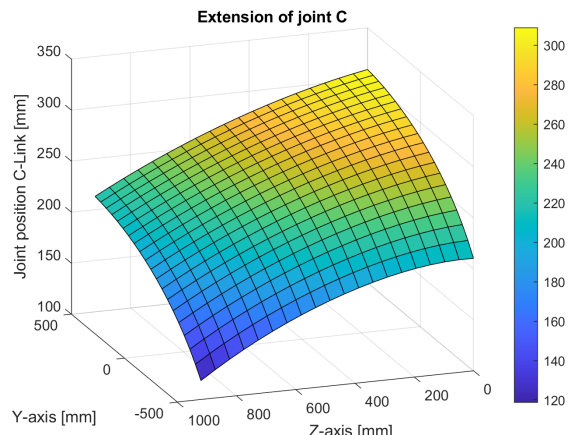


Figure A.35: Joint position at C2 for extending links concept at 60° head angle

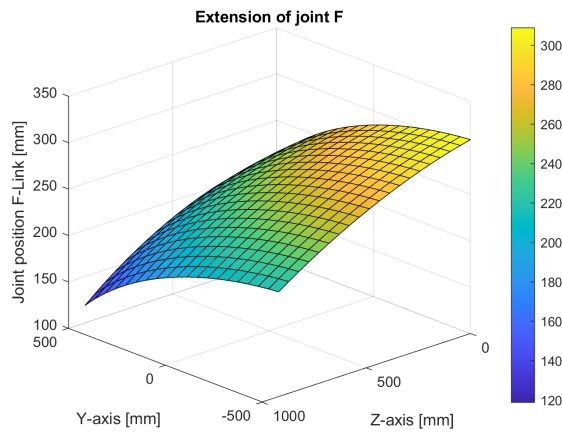


Figure A.36: Joint position at F2 for extending links concept at 60° head angle

## A.7 70 Degrees

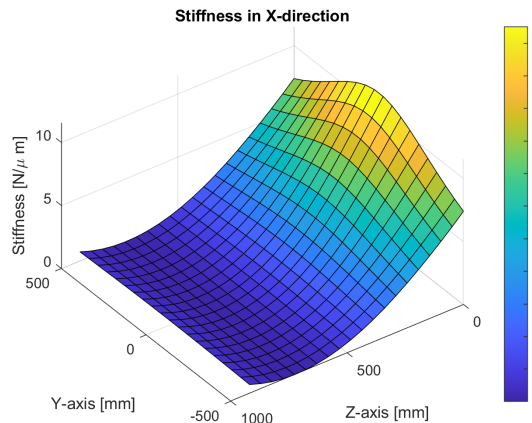


Figure A.37: Stiffness for load in X-direction for extending links concept at 70° head angle

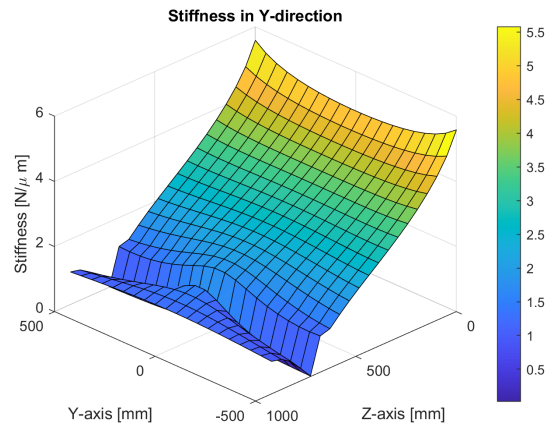


Figure A.38: Stiffness for load in Y-direction for extending links concept at 70° head angle

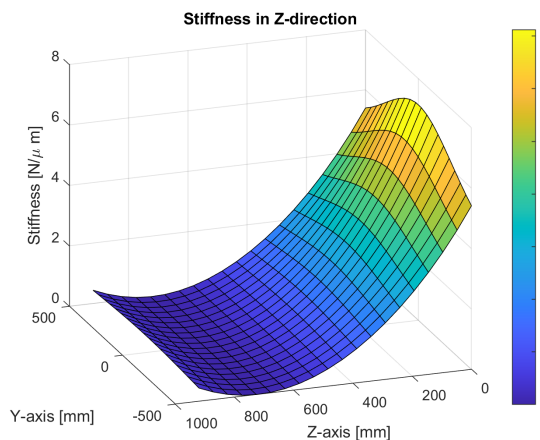


Figure A.39: Stiffness for load in Z-direction for extending links concept at 70° head angle

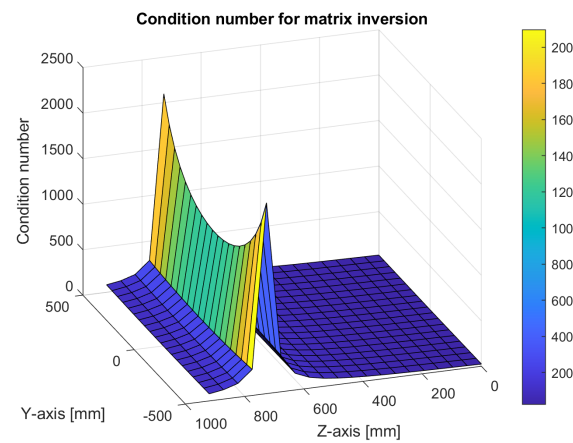


Figure A.40: Condition number for matrix inversion for extending links concept at 70° head angle

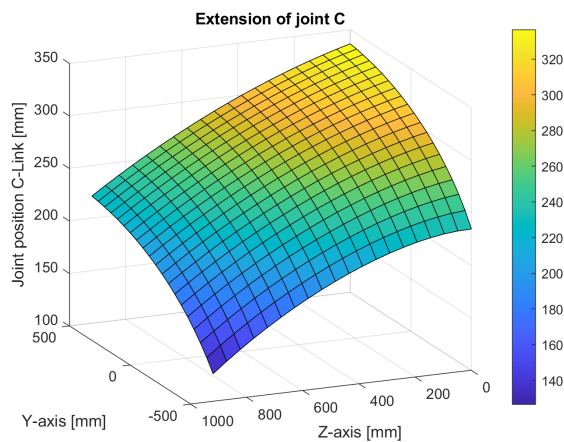


Figure A.41: Joint position at C2 for extending links concept at 70° head angle

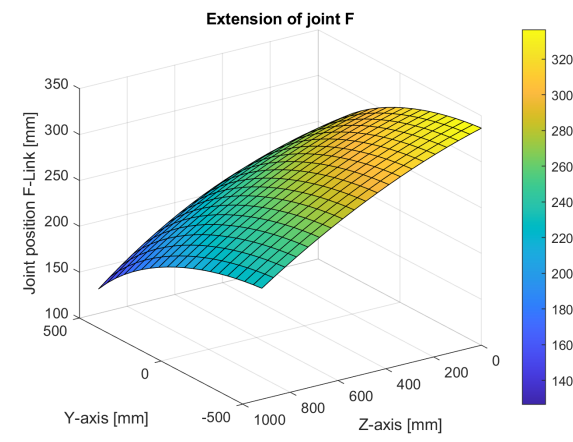


Figure A.42: Joint position at F2 for extending links concept at 70° head angle

## A.8 80 Degrees

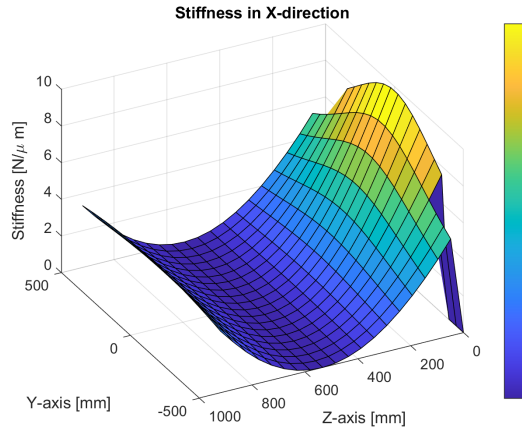


Figure A.43: Stiffness for load in X-direction for extending links concept at 80° head angle

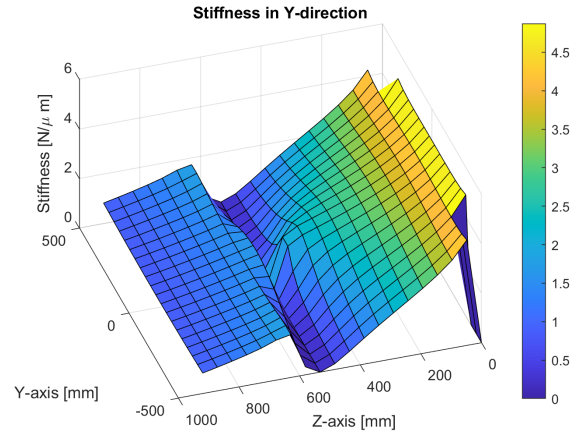


Figure A.44: Stiffness for load in Y-direction for extending links concept at 80° head angle

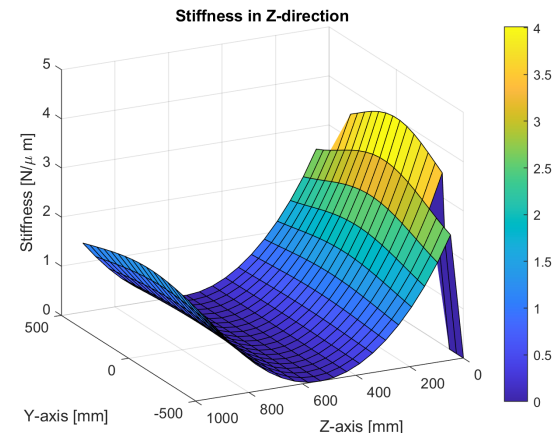


Figure A.45: Stiffness for load in Z-direction for extending links concept at 80° head angle

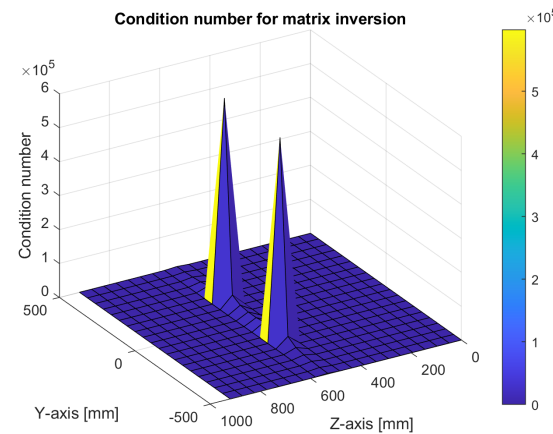


Figure A.46: Condition number for matrix inversion for extending links concept at 80° head angle

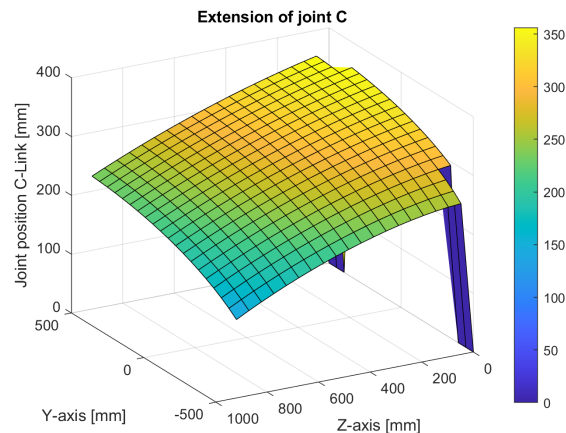


Figure A.47: Joint position at C2 for extending links concept at 80° head angle

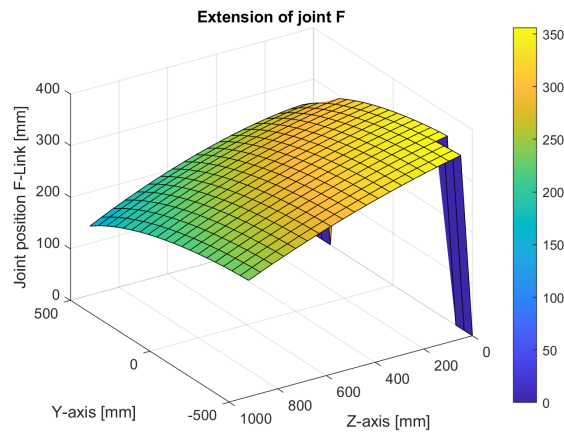


Figure A.48: Joint position at F2 for extending links concept at 80° head angle

## A.9 90 Degrees

Figure A.49: Stiffness for load in X-direction for extending links concept at 90° head angle

Figure A.50: Stiffness for load in Y-direction for extending links concept at 90° head angle

Figure A.51: Stiffness for load in Z-direction for extending links concept at 90° head angle

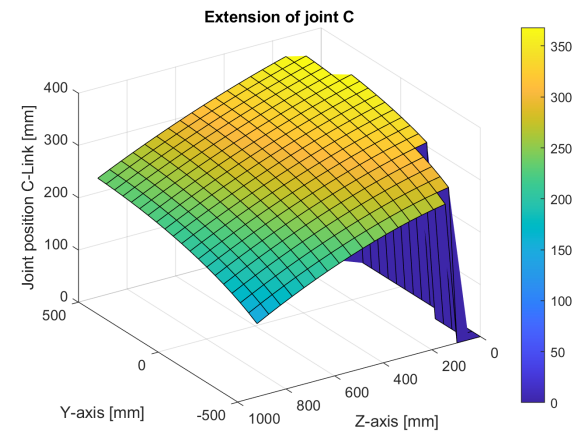


Figure A.53: Joint position at C2 for extending links concept at 90° head angle

Figure A.52: Condition number for matrix inversion for extending links concept at 90° head angle

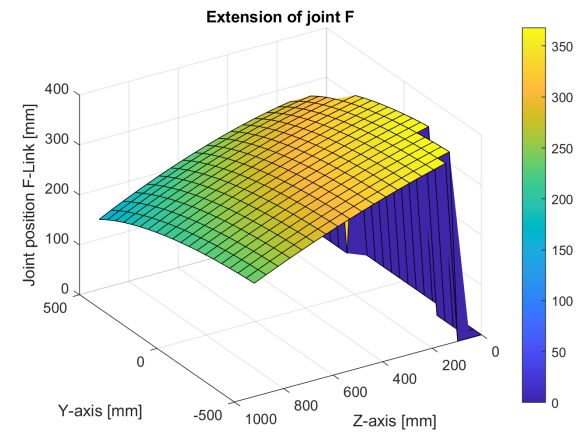


Figure A.54: Joint position at F2 for extending links concept at 90° head angle

## Appendix B

# Stiffness graphs for rotational sleds concept

### B.1 10 Degrees

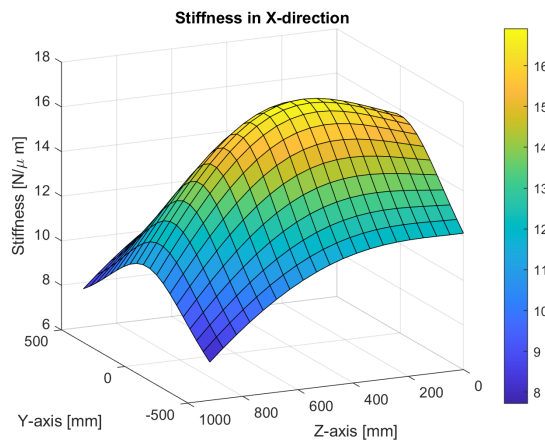


Figure B.1: Stiffness for rotational sled concept for load in X-direction at 10° head angle

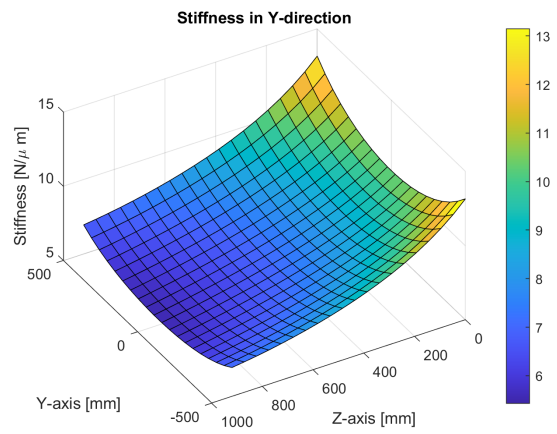


Figure B.2: Stiffness for rotational sled concept for load in Y-direction at 10° head angle

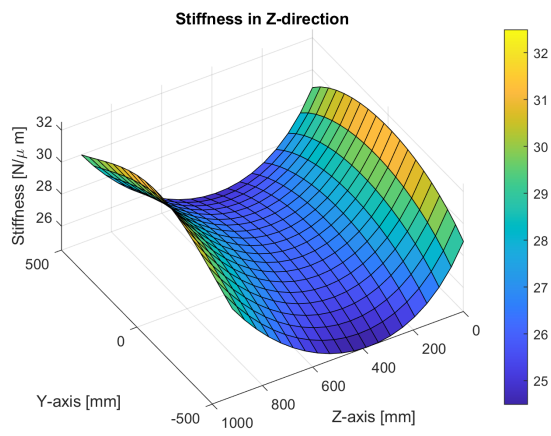


Figure B.3: Stiffness for rotational sled concept for load in Z-direction at 10° head angle

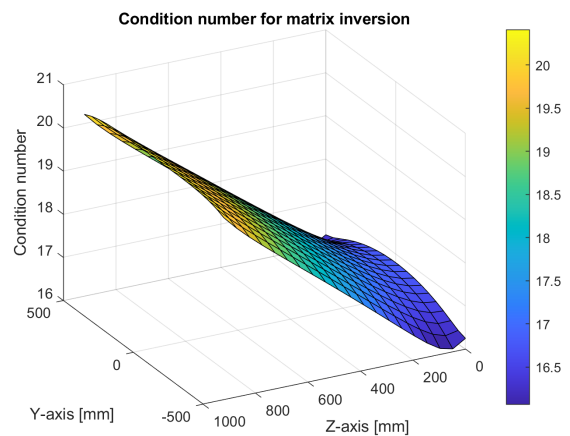


Figure B.4: Rotational sled concept condition number for matrix inversion at 10° head angle

## B.2 20 Degrees

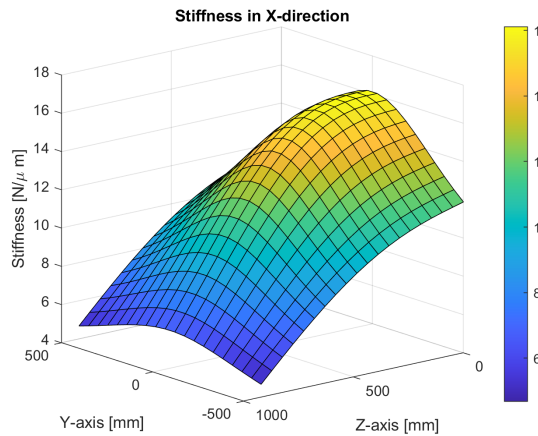


Figure B.5: Stiffness for rotational sled concept for load in X-direction at 20° head angle

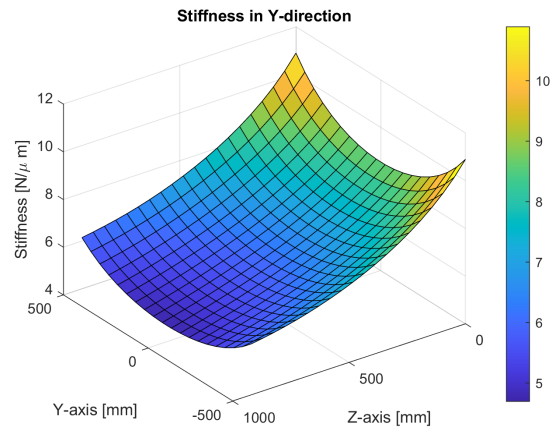


Figure B.6: Stiffness for rotational sled concept for load in Y-direction at 20° head angle

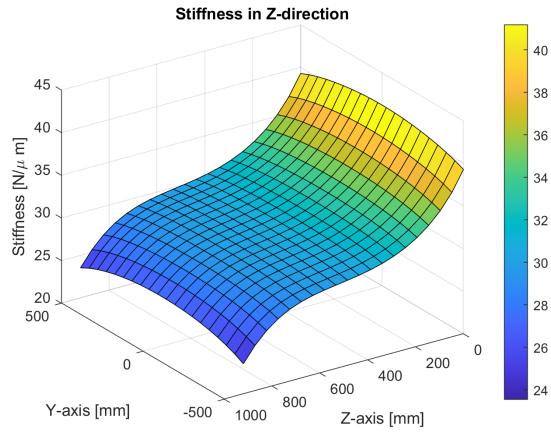


Figure B.7: Stiffness for rotational sled concept for load in Z-direction at 20° head angle

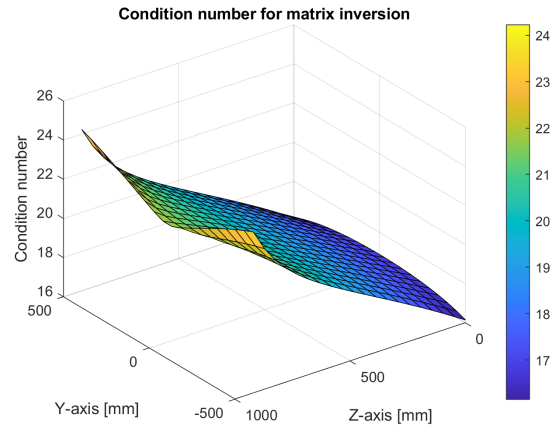


Figure B.8: Rotational sled concept condition number for matrix inversion at 20° head angle

### B.3 30 Degrees

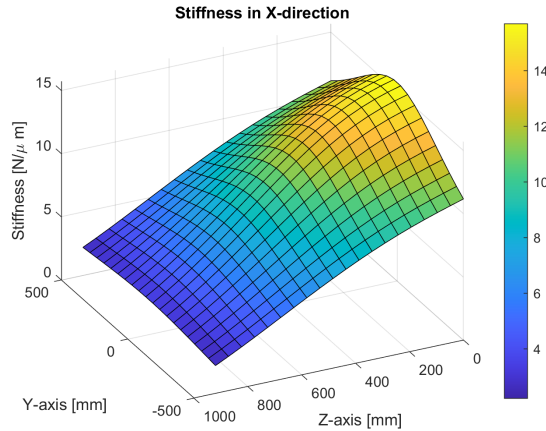


Figure B.9: Stiffness for rotational sled concept for load in X-direction at  $30^\circ$  head angle

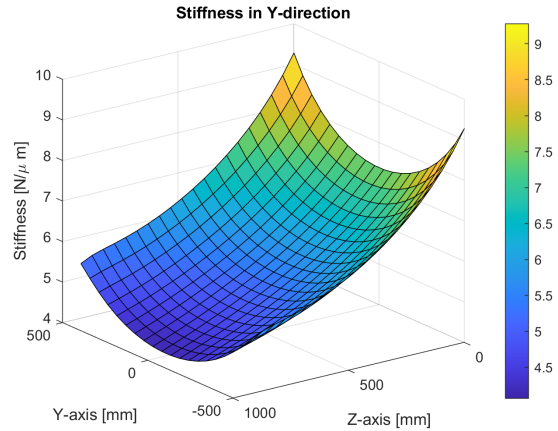


Figure B.10: Stiffness for rotational sled concept for load in Y-direction at  $30^\circ$  head angle

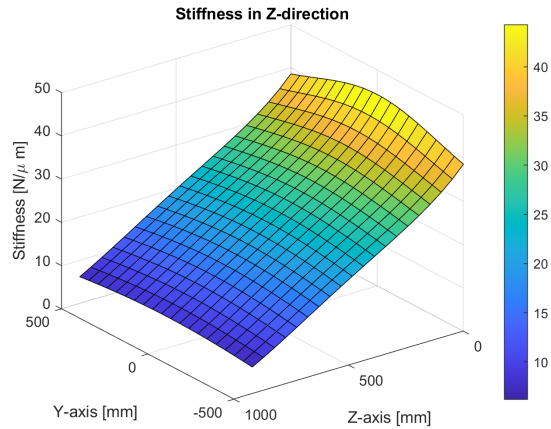


Figure B.11: Stiffness for rotational sled concept for load in Z-direction at  $30^\circ$  head angle

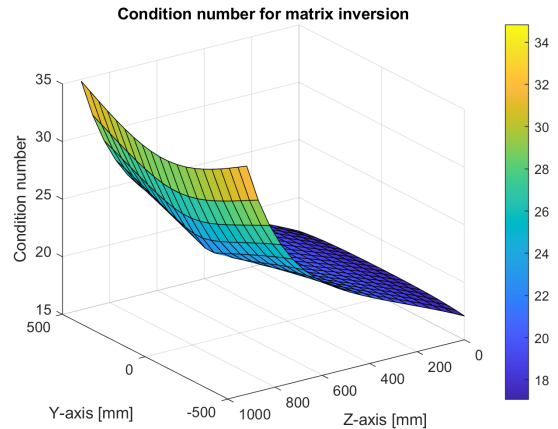


Figure B.12: Rotational sled concept condition number for matrix inversion at  $30^\circ$  head angle

## B.4 40 Degrees

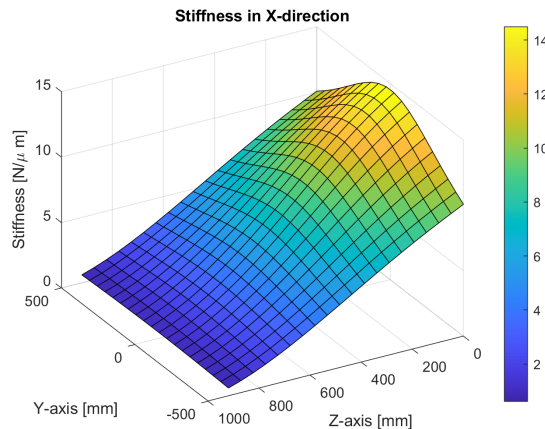


Figure B.13: Stiffness for rotational sled concept for load in X-direction at 40° head angle

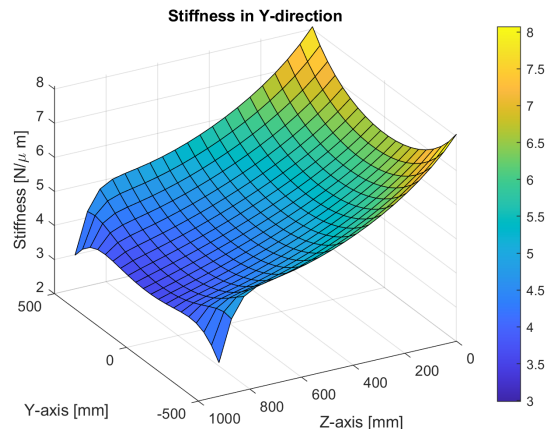


Figure B.14: Stiffness for rotational sled concept for load in Y-direction at 40° head angle

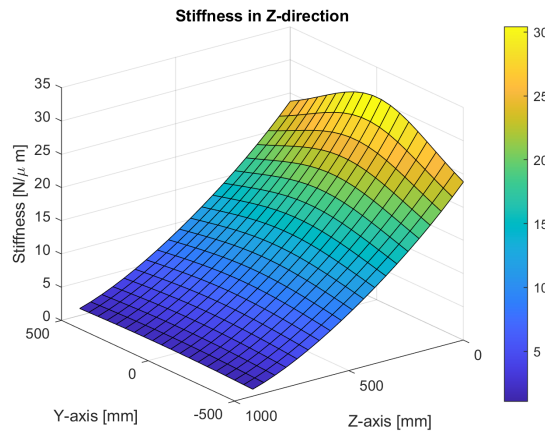


Figure B.15: Stiffness for rotational sled concept for load in Z-direction at 40° head angle

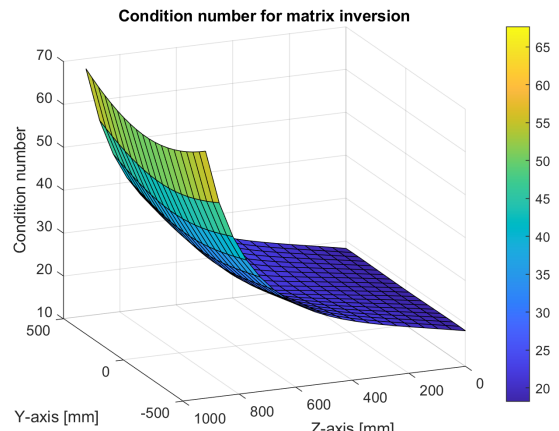


Figure B.16: Rotational sled concept condition number for matrix inversion at 40° head angle

## B.5 50 Degrees

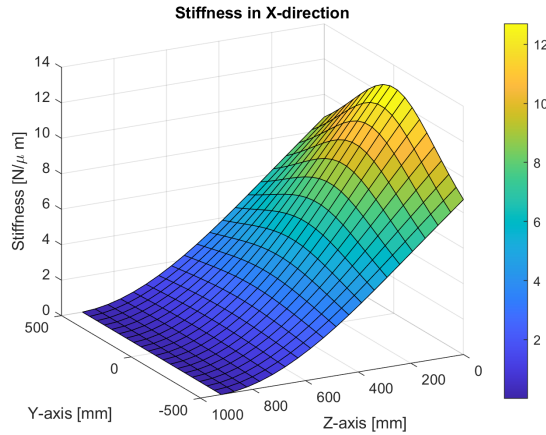


Figure B.17: Stiffness for rotational sled concept for load in X-direction at  $50^\circ$  head angle

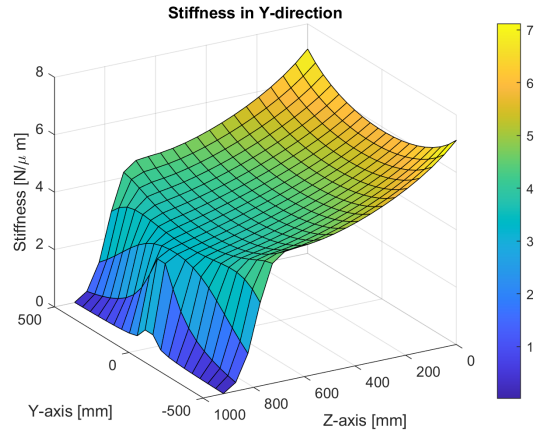


Figure B.18: Stiffness for rotational sled concept for load in Y-direction at  $50^\circ$  head angle

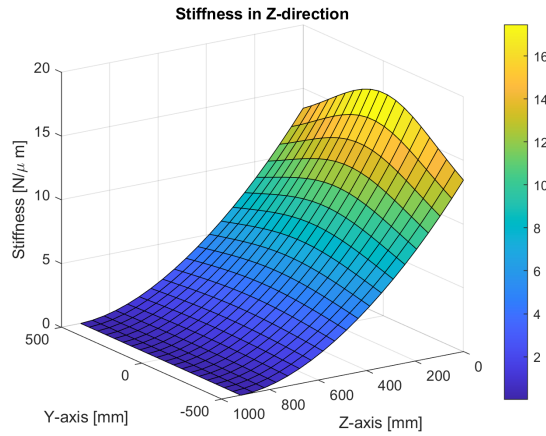


Figure B.19: Stiffness for rotational sled concept for load in Z-direction at  $50^\circ$  head angle

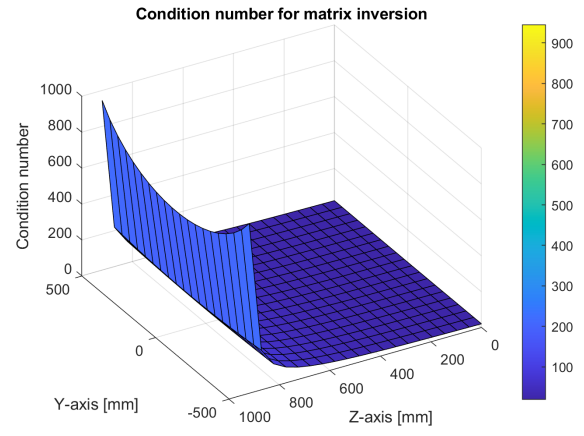


Figure B.20: Rotational sled concept condition number for matrix inversion at  $50^\circ$  head angle

## B.6 60 Degrees

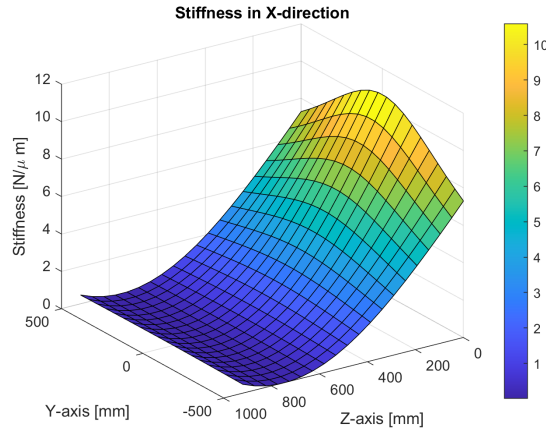


Figure B.21: Stiffness for rotational sled concept for load in X-direction at  $60^\circ$  head angle

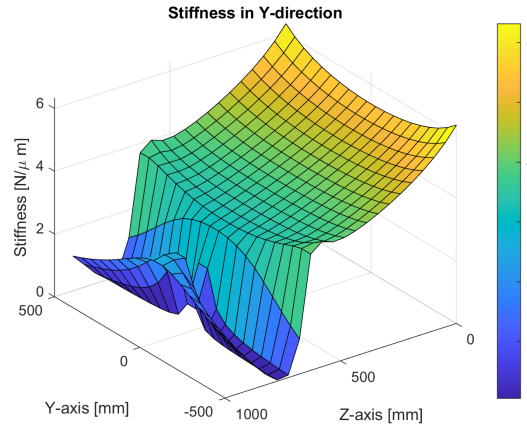


Figure B.22: Stiffness for rotational sled concept for load in Y-direction at  $60^\circ$  head angle

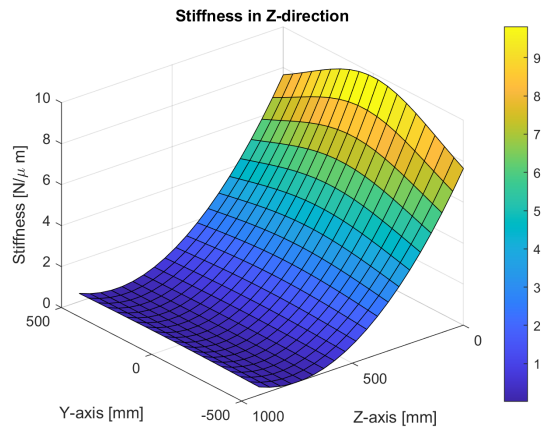


Figure B.23: Stiffness for rotational sled concept for load in Z-direction at  $60^\circ$  head angle

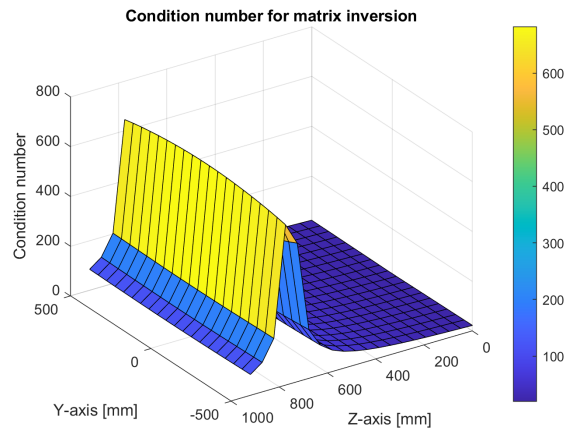


Figure B.24: Rotational sled concept condition number for matrix inversion at  $60^\circ$  head angle

## B.7 70 Degrees

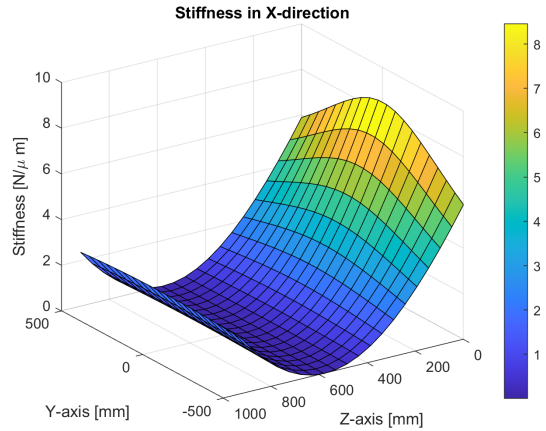


Figure B.25: Stiffness for rotational sled concept for load in X-direction at  $70^\circ$  head angle

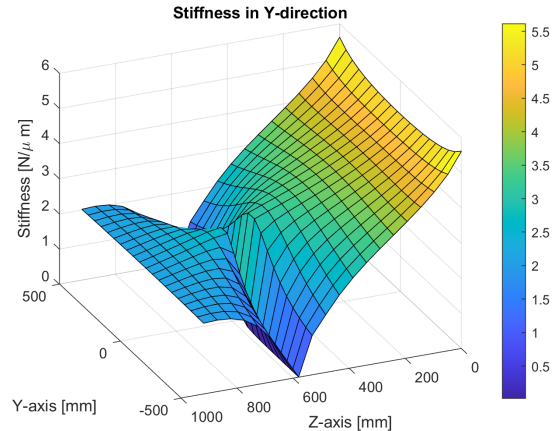


Figure B.26: Stiffness for rotational sled concept for load in Y-direction at  $70^\circ$  head angle

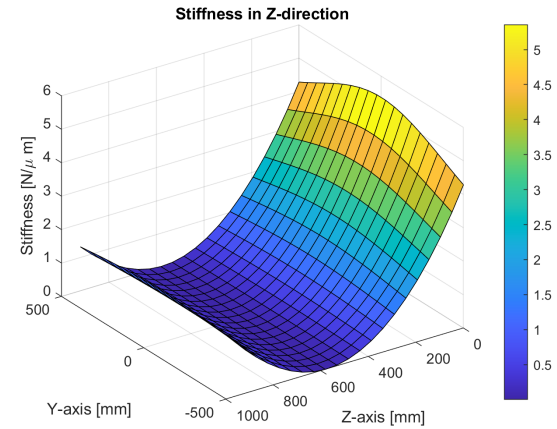


Figure B.27: Stiffness for rotational sled concept for load in Z-direction at  $70^\circ$  head angle

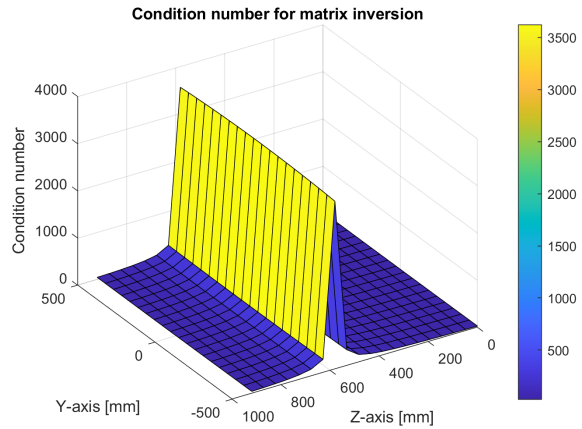


Figure B.28: Rotational sled concept condition number for matrix inversion at  $70^\circ$  head angle

## B.8 80 Degrees

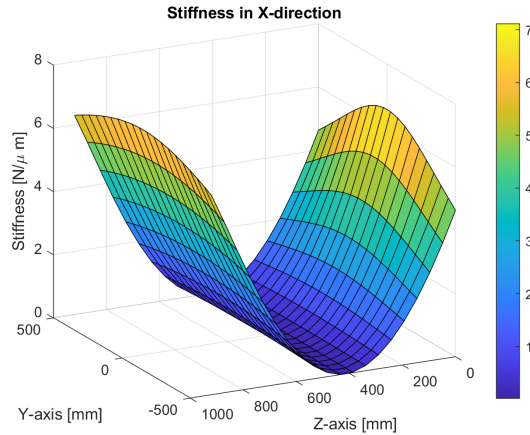


Figure B.29: Stiffness for rotational sled concept for load in X-direction at 80° head angle

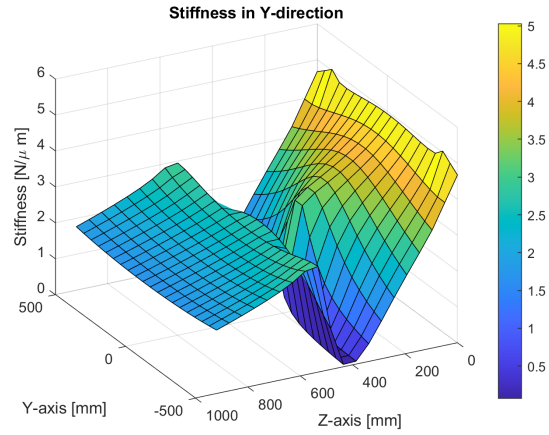


Figure B.30: Stiffness for rotational sled concept for load in Y-direction at 80° head angle

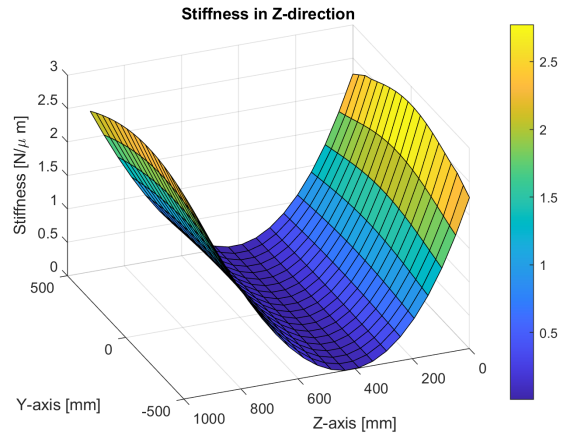


Figure B.31: Stiffness for rotational sled concept for load in Z-direction at 80° head angle

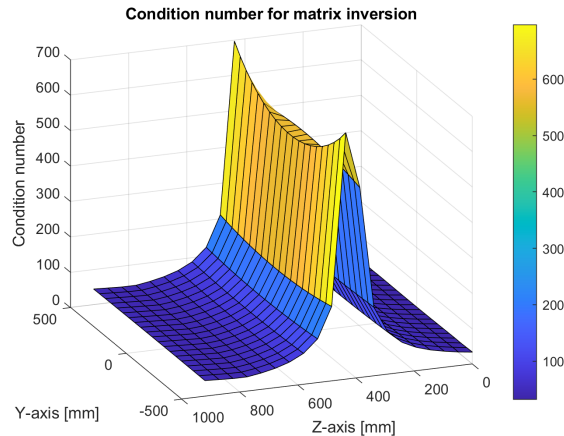


Figure B.32: Rotational sled concept condition number for matrix inversion at 80° head angle

## B.9 90 Degrees

Figure B.33: Stiffness for rotational sled concept  
for load in X-direction at 90° head angle

Figure B.34: Stiffness for rotational sled concept  
for load in Y-direction at 90° head angle

Figure B.35: Stiffness for rotational sled concept  
for load in Z-direction at 90° head angle

Figure B.36: Rotational sled concept condition  
number for matrix inversion at 90° head angle

## Appendix C

# Stiffness graphs for delta light concept

### C.1 10 Degrees

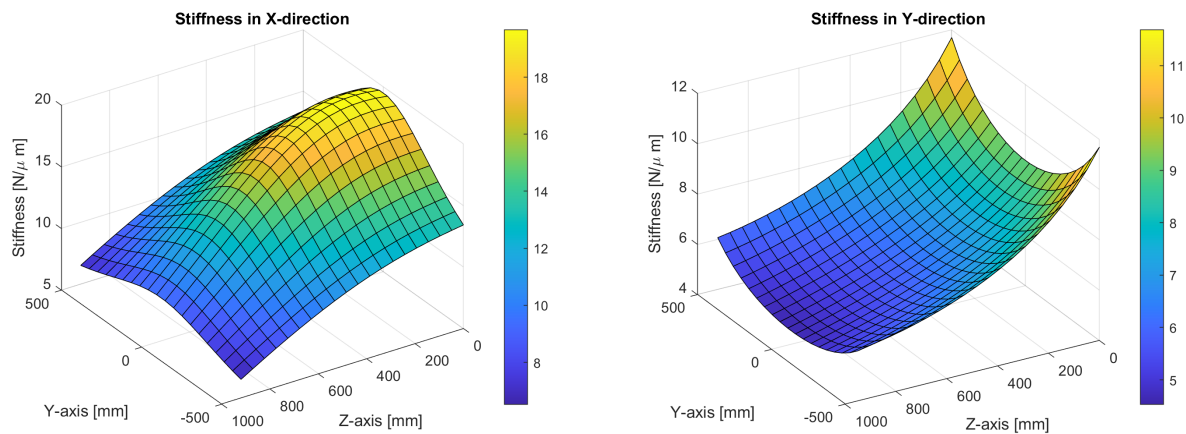


Figure C.1: Stiffness for delta light concept for load in X-direction at  $10^\circ$  head angle

Figure C.2: Stiffness for delta light concept for load in Y-direction at  $10^\circ$  head angle

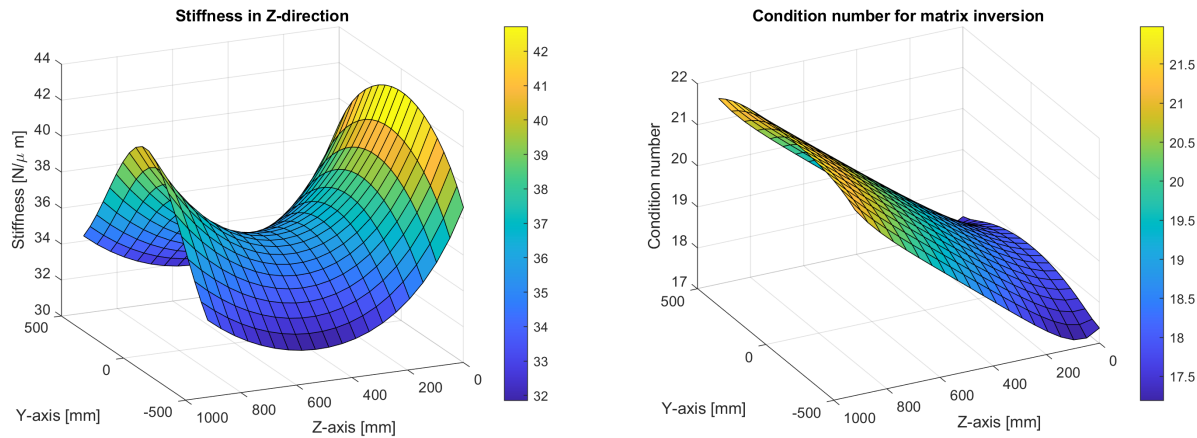


Figure C.3: Stiffness for delta light concept for load in Z-direction at  $10^\circ$  head angle

Figure C.4: Delta light concept condition number for matrix inversion at  $10^\circ$  head angle

## C.2 20 Degrees

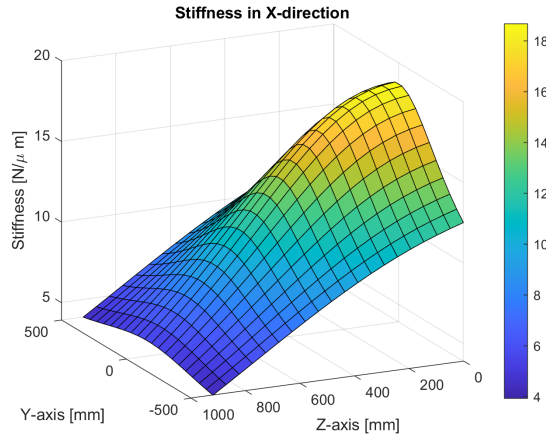


Figure C.5: Stiffness for delta light concept for load in X-direction at  $20^\circ$  head angle

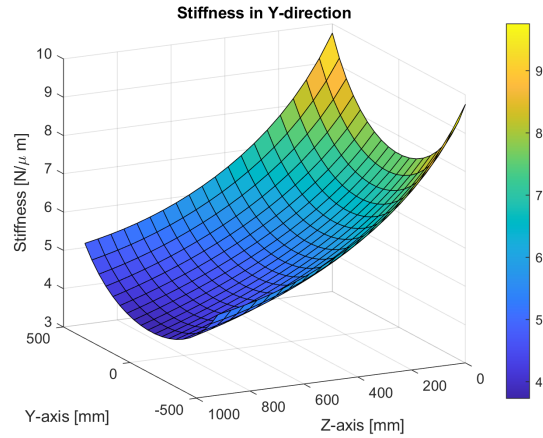


Figure C.6: Stiffness for delta light concept for load in Y-direction at  $20^\circ$  head angle

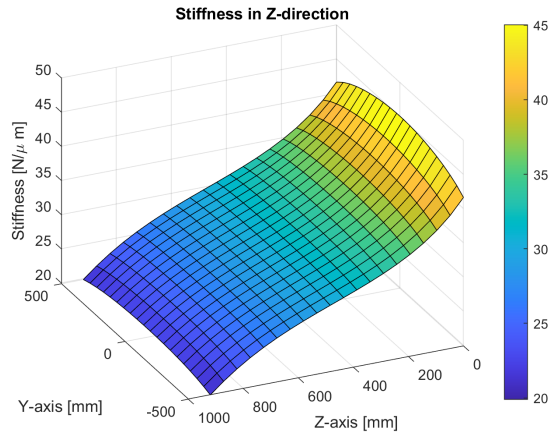


Figure C.7: Stiffness for delta light concept for load in Z-direction at  $20^\circ$  head angle

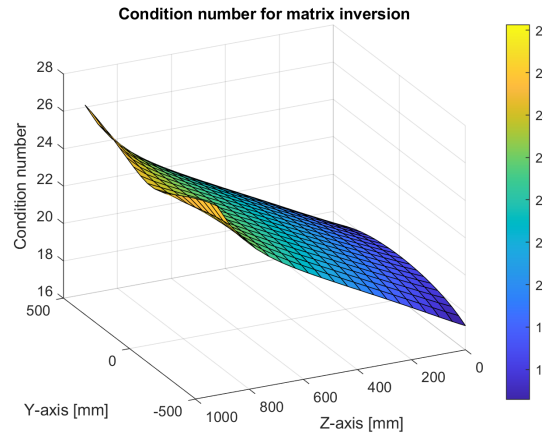


Figure C.8: Delta light concept condition number for matrix inversion at  $20^\circ$  head angle

### C.3 30 Degrees

Figure C.9: Stiffness for delta light concept for load in X-direction at 30° head angle

Figure C.10: Stiffness for delta light concept for load in Y-direction at 30° head angle

Figure C.11: Stiffness for delta light concept for load in Z-direction at 30° head angle

Figure C.12: Delta light concept condition number for matrix inversion at 30° head angle

## C.4 40 Degrees

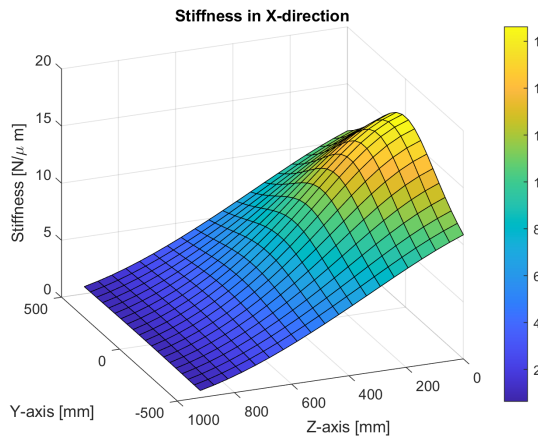


Figure C.13: Stiffness for delta light concept for load in X-direction at 40° head angle

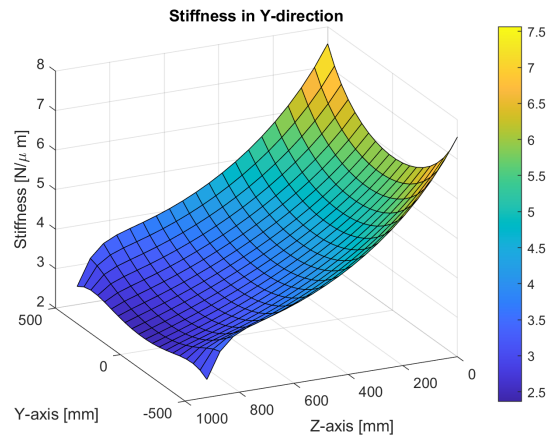


Figure C.14: Stiffness for delta light concept for load in Y-direction at 40° head angle

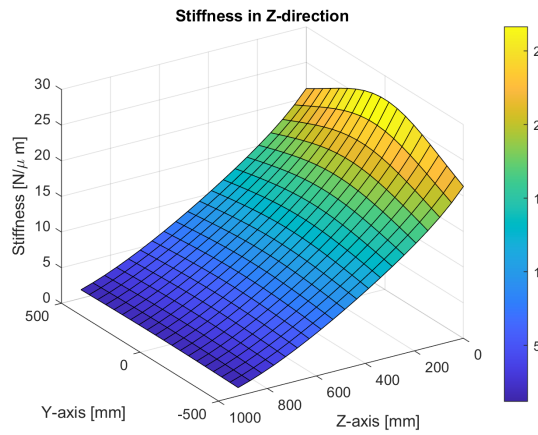


Figure C.15: Stiffness for delta light concept for load in Z-direction at 40° head angle

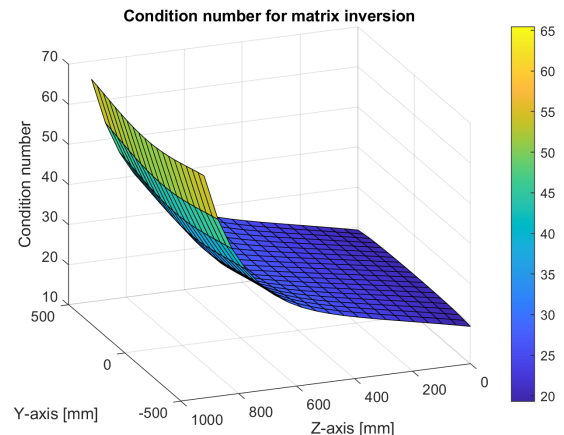


Figure C.16: Delta light concept condition number for matrix inversion at 40° head angle

## C.5 50 Degrees

Figure C.17: Stiffness for delta light concept for load in X-direction at 50° head angle

Figure C.18: Stiffness for delta light concept for load in Y-direction at 50° head angle

Figure C.19: Stiffness for delta light concept for load in Z-direction at 50° head angle

Figure C.20: Delta light concept condition number for matrix inversion at 50° head angle

## C.6 60 Degrees

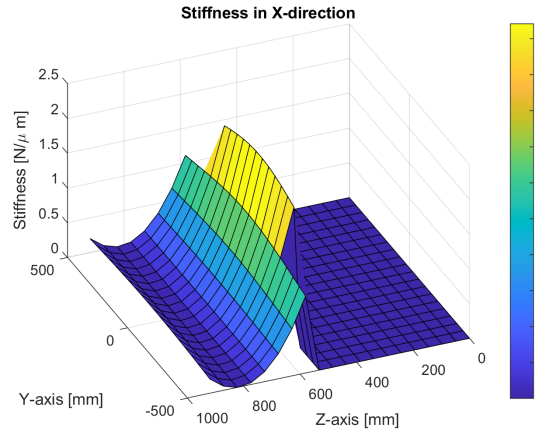


Figure C.21: Stiffness for delta light concept for load in X-direction at  $60^\circ$  head angle

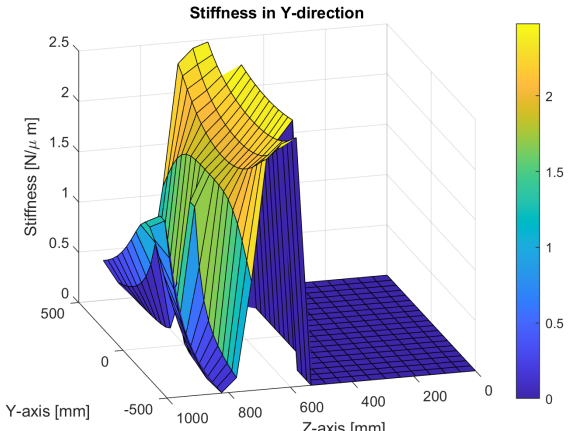


Figure C.22: Stiffness for delta light concept for load in Y-direction at  $60^\circ$  head angle

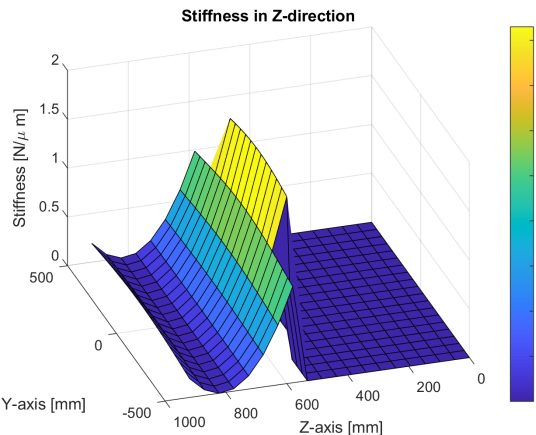


Figure C.23: Stiffness for delta light concept for load in Z-direction at  $60^\circ$  head angle

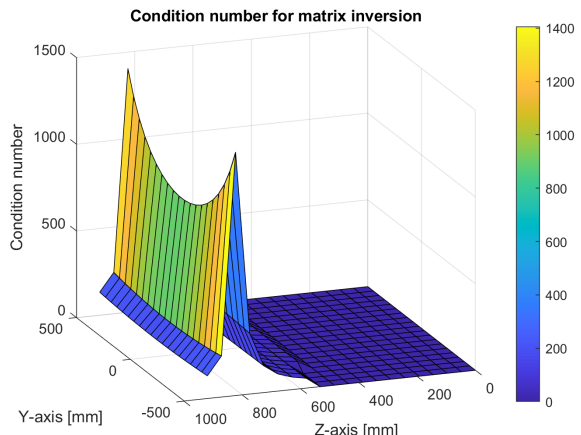


Figure C.24: Delta light concept condition number for matrix inversion at  $60^\circ$  head angle

## Appendix D

### Stiffness graphs for double sled concept

## D.1 10 Degrees

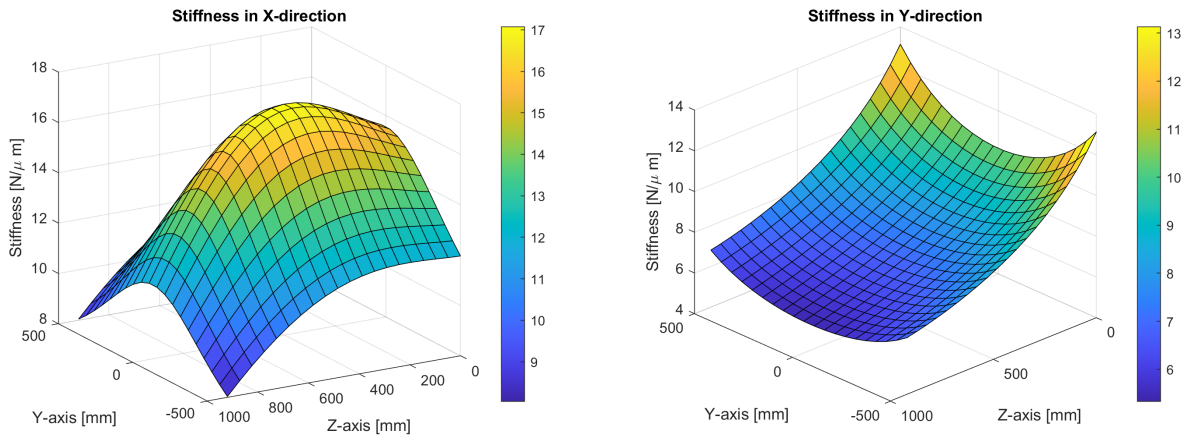


Figure D.1: Stiffness for double sled for load in X-direction at  $10^\circ$  head angle

Figure D.2: Stiffness for double sled for load in Y-direction at  $10^\circ$  head angle

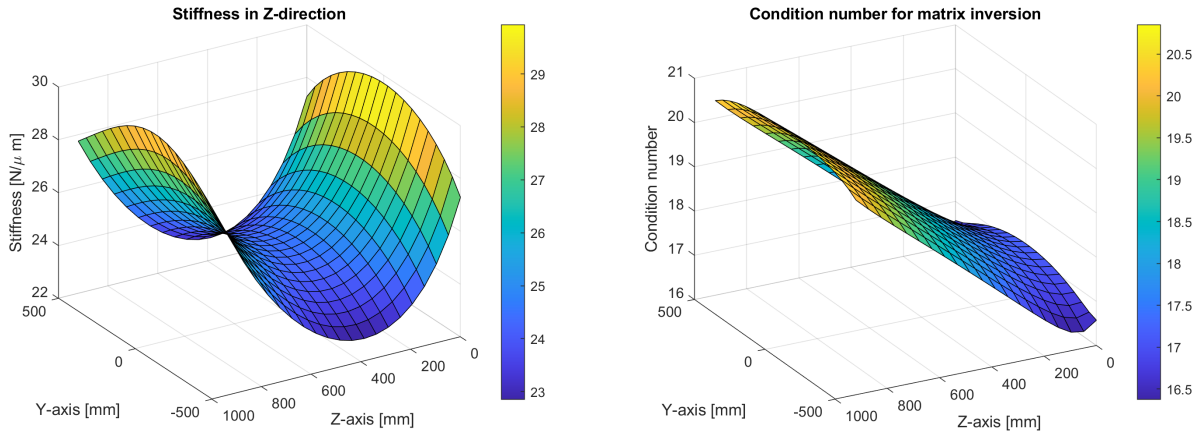


Figure D.3: Stiffness for double sled for load in Z-direction at  $10^\circ$  head angle

Figure D.4: Double sled condition number for matrix inversion at  $10^\circ$  head angle

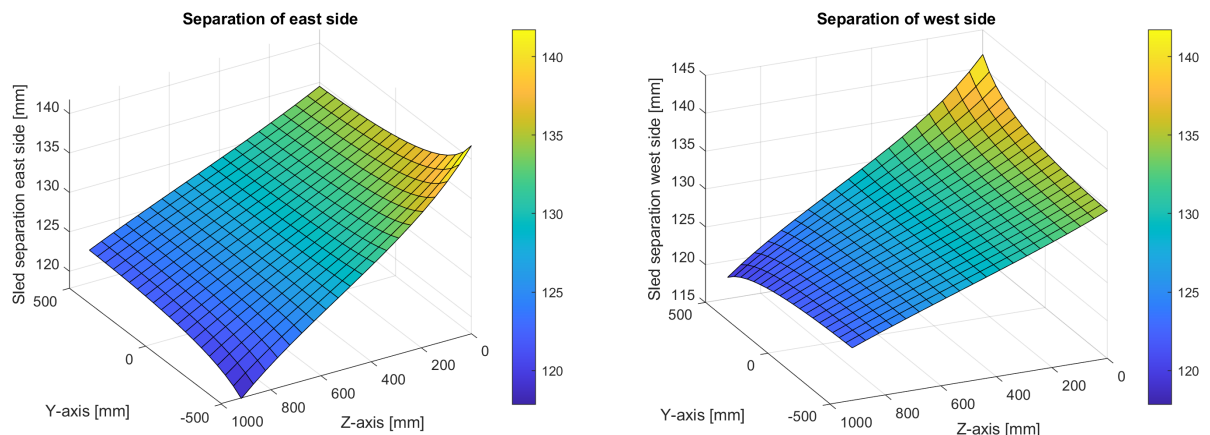


Figure D.5: Necessary sled separation at  $10^\circ$  head angle

Figure D.6: Necessary sled separation at  $10^\circ$  head angle

## D.2 20 Degrees

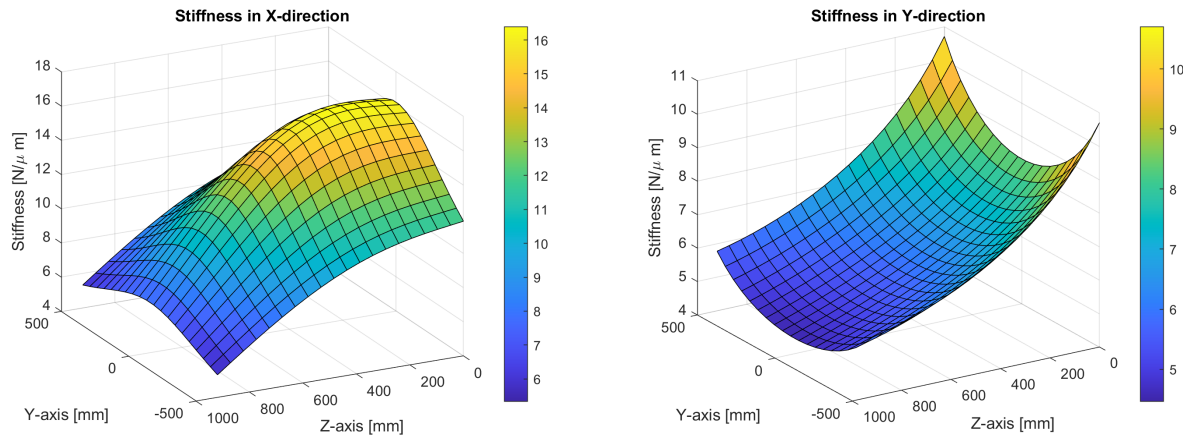


Figure D.7: Stiffness for double sled for load in X-direction at  $20^\circ$  head angle

Figure D.8: Stiffness for double sled for load in Y-direction at  $20^\circ$  head angle

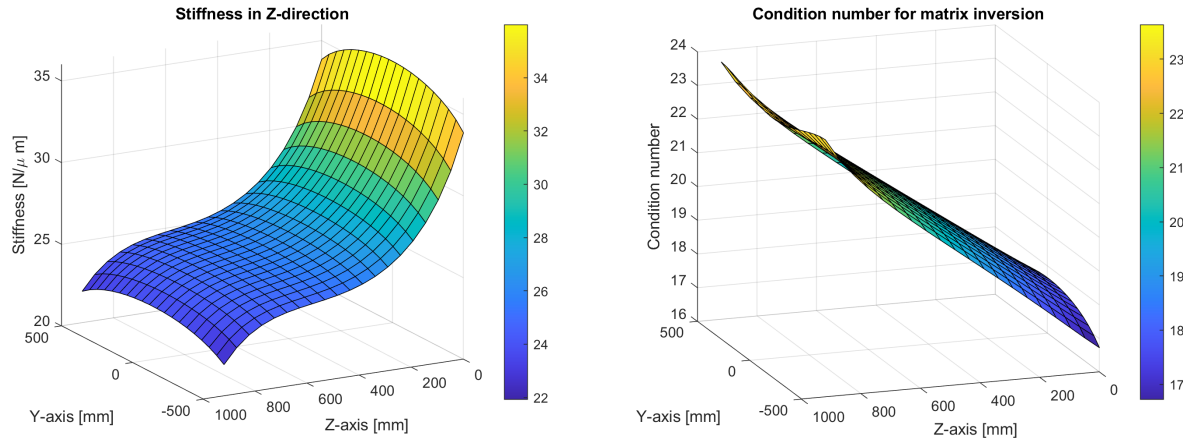


Figure D.9: Stiffness for double sled for load in Z-direction at  $20^\circ$  head angle

Figure D.10: Double sled condition number for matrix inversion at  $20^\circ$  head angle

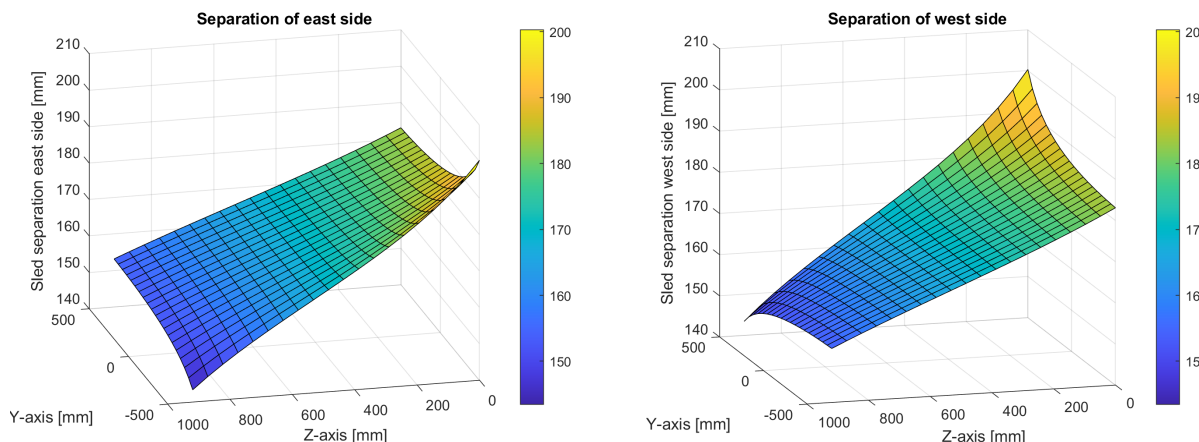


Figure D.11: Necessary sled separation at  $20^\circ$  head angle

Figure D.12: Necessary sled separation at  $20^\circ$  head angle

### D.3 30 Degrees

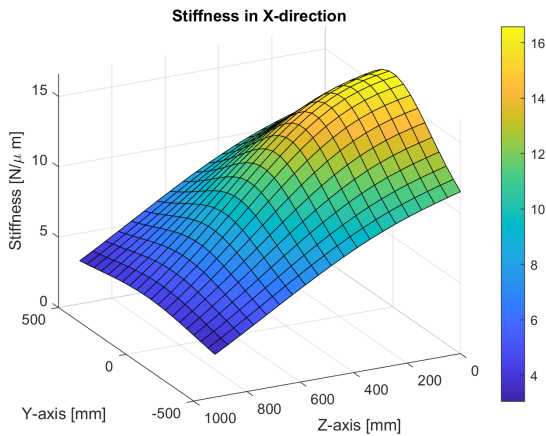


Figure D.13: Stiffness for double sled for load in X-direction at  $30^\circ$  head angle

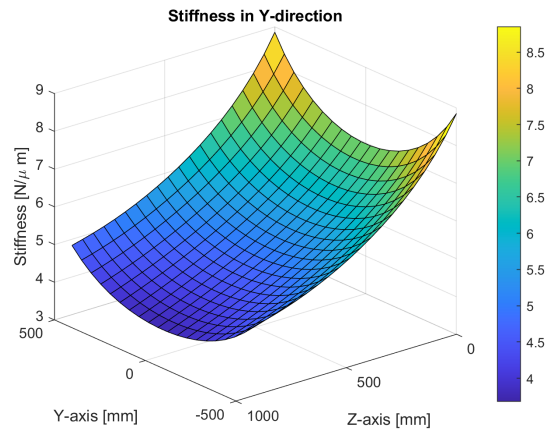


Figure D.14: Stiffness for double sled for load in Y-direction at  $30^\circ$  head angle

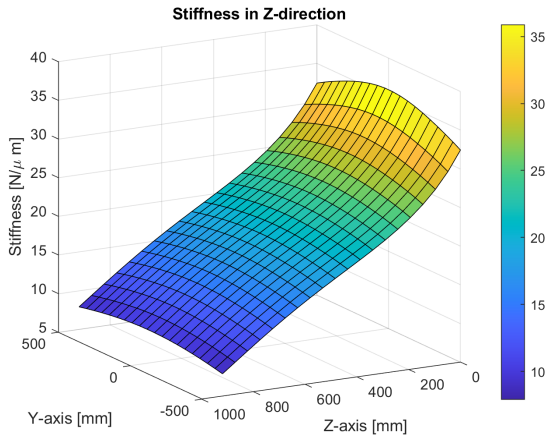


Figure D.15: Stiffness for double sled for load in Z-direction at  $30^\circ$  head angle

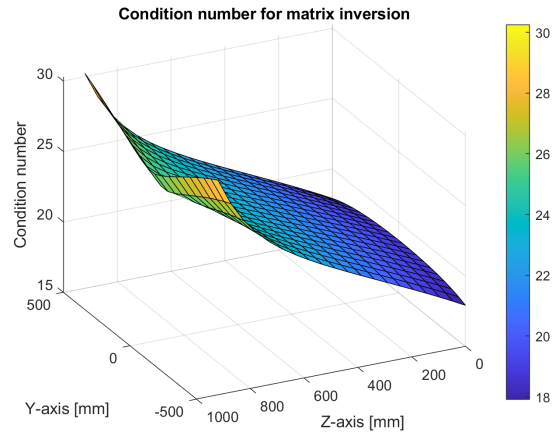


Figure D.16: Double sled condition number for matrix inversion at  $30^\circ$  head angle

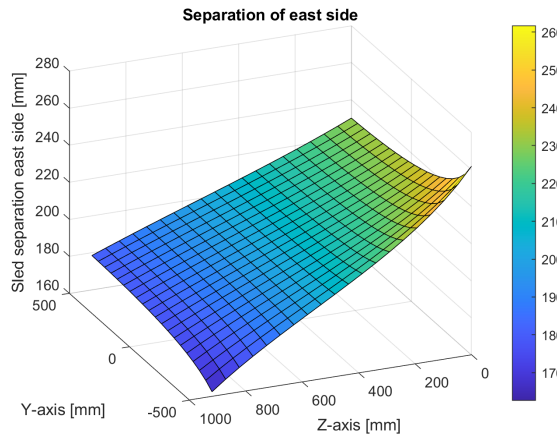


Figure D.17: Necessary sled separation at  $30^\circ$  head angle

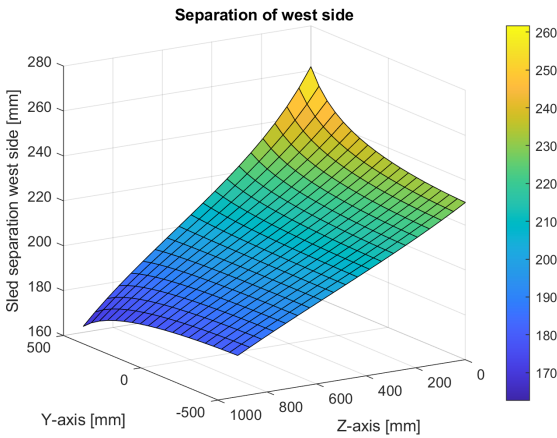


Figure D.18: Necessary sled separation at  $30^\circ$  head angle

## D.4 40 Degrees

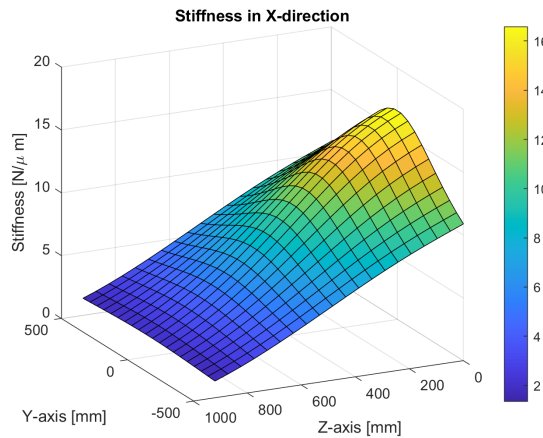


Figure D.19: Stiffness for double sled for load in X-direction at 40° head angle

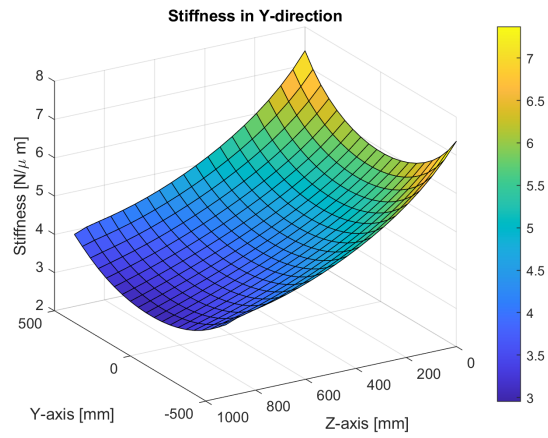


Figure D.20: Stiffness for double sled for load in Y-direction at 40° head angle

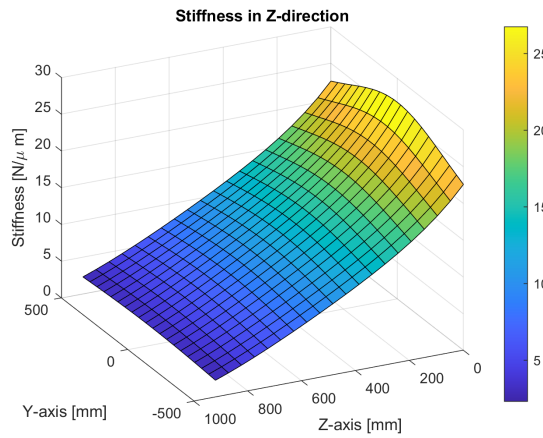


Figure D.21: Stiffness for double sled for load in Z-direction at 40° head angle

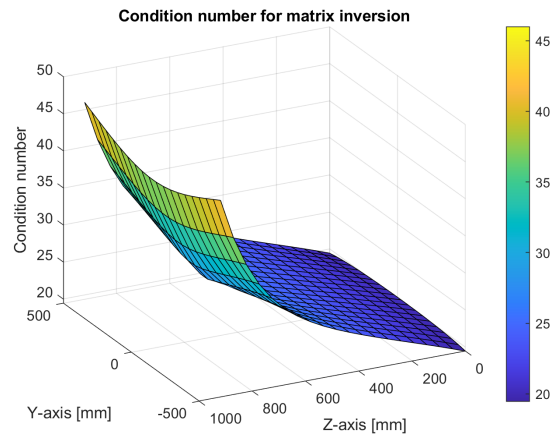


Figure D.22: Double sled condition number for matrix inversion at 40° head angle

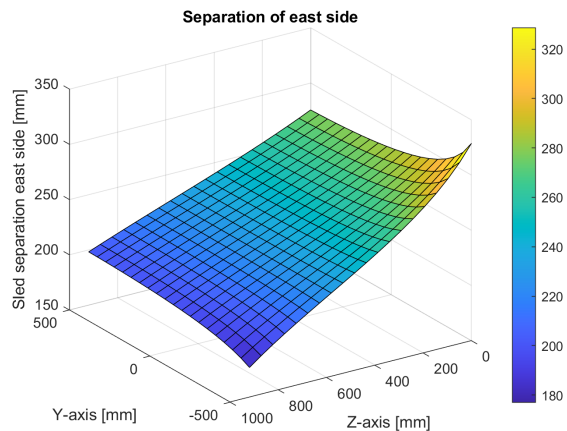


Figure D.23: Necessary sled separation at 40° head angle

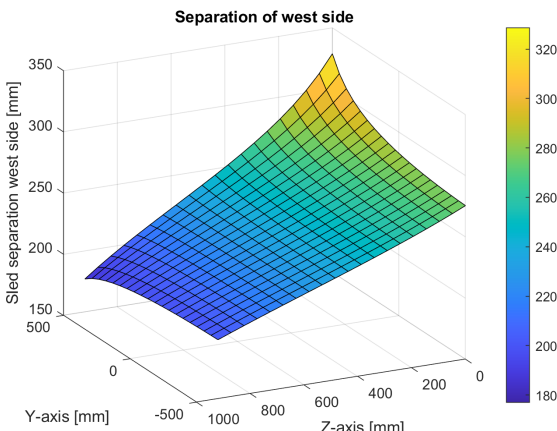


Figure D.24: Necessary sled separation at 40° head angle